Effects of atmospheric CO_2 level on the metabolic response of resistant and susceptible wheat to *Fusarium graminearum* infection

Miroslava Cuperlovic-Culf[1*+], Martha M. Vaughan[2*], Karl Vermillion[2], Anu Surendra[1], Jennifer Teresi[2], Susan P. McCormick[2].

[1]National Research Council Canada, Ottawa, Canada

[2]Mycotoxin Prevention and Applied Microbiology Research Unit, NCAUR, USDA-ARS, Peoria, IL, USA.

*contributed equally to this publication

+ To whom correspondence should be addressed.

Miroslava Cuperlovic-Culf, National Research Council, 1200 Montreal Road, Ottawa, ON K1A 0R6, Canada

Tel: 6139930116; Fax: 6139520315; Email: miroslava.cuperlovic-culf@nrc-cnrc.gc.ca

Abstract

Rising atmospheric CO_2 concentration and associated climate changes are thought to have contributed to the steady increase of Fusarium head blight (FHB) on wheat. However, our understanding of precisely how elevated CO_2 influences the defense response of wheat against *Fusarium graminearum (Fg)* remains limited. In this study, we evaluated the metabolic profiles of susceptible (Norm) and moderately resistant (Alsen) spring wheat in response to whole-head inoculation with two deoxynivalenol (DON) producing *Fg* isolates (DON^+) *Fg* isolates (9F1 and Gz3639), and a DON deficient (DON^-) *Fg* isolate (Gzt40) at ambient (400ppm) and elevated (800ppm) CO_2 concentrations. The effects of elevated CO_2 were dependent on both the *Fg* strain and the wheat variety, but metabolic differences in the host can explain the observed changes in *Fg* biomass and DON accumulation. The complexity of abiotic and biotic stress interactions make it difficult to determine if the observed metabolic changes in wheat are a result of CO_2 induced changes in the host, the pathogen, or a combination of both. However, the effects of elevated CO_2 were not dependent on DON production. Finally, we identified several metabolic biomarkers for wheat that can reliably predict FHB resistance or susceptibility even as atmospheric CO_2 levels rise.

Introduction

The global average atmospheric carbon dioxide (CO_2) concentration surpassed 400 ppm in 2016 and is rising at an unprecedented pace (NOAA, 2017). By 2100, the CO_2 concentration is predicted to reach 800 ppm, contributing to significant climate changes (Stocker et al., 2013). The Average global temperature is expected to rise 2 to 4°C and seasonal and regional climate

conditions will very likely become more variable and extreme (Stocker et al., 2013). In the Great Plains where most of the US wheat is produced, while the frequency and intensity of heat waves and drought are predicted to increase in the south, the northern states are expected to have increased precipitation and heavy downpours (Barton and Clark, 2014).

Climate directly impacts the growth, development, and productivity of agricultural crops, as well as the frequency and severity of disease epidemics. Elevated CO_2 has been shown to increase wheat growth, flowering time, maturation and yield, but also reduces grain nutritional quality and alters plant primary and secondary metabolism (Hogy et al. 2009). All of these changes have to potential to influence plant susceptibility pathogens. This is concerning because future climate conditions are also projected to increase the geographic distribution, growth rate, and virulence of major agricultural pathogens. Crop-destroying fungal pathogens, in particular, are expected to be amongst the greatest threat to future global food security (Fisher et al., 2012; Bebber 2015; Bebber and Gurr, 2015).

Fusarium head blight (FHB) is one of the most devastating fungal diseases of wheat. FHB can be caused by a number of closely related fungal species, but in many regions of the world *Fusarium graminearum* (*Fg*) is the primary etiological agent. FHB epidemics substantially reduce grain yield and quality, and contaminate grain with harmful trichothecene mycotoxins that can render the grain unsafe for human or animal consumption. Trichothecenes are a serious food safety concern because they inhibit protein synthesis and cause neurologic, gastrointestinal and immune function disorders (Pestka, 2010; Wu et al., 2014). However, trichothecene production, especially the production of deoxynivalenol (DON), is an important virulence factor allowing the

pathogen to overcome the plant's defenses and spread throughout the host (Mesterhazy et al. 1999; Bai et al., 2002). Over the past few decades, *Fg* has caused widespread outbreaks of FHB resulting in significant economic losses to the wheat industry (Dweba et al., 2017). The prevalence of FHB and highly DON contaminated grain has increased in recent years due to changes in climate and agricultural practices (Edwards, 2004; Fisher et al., 2012; Kane et al., 2013). FHB epidemics and DON contamination of grain are strongly associated with climate, and occur when wheat anthesis coincides with warm wet conditions. The frequency of such favorable conditions for disease is projected to increase in the future with climate change intensifying the risk of FHB and mycotoxin food safety issues (Chakraborty and Newton, 2011; Madgwick et al., 2011; Zhang et al., 2014; Vaughan et al., 2016).

Two main types of wheat resistance to FHB are: (type I) resistance to initial infection, which is typically evaluated by the incidence of infected florets following whole-head inoculation, and (type II) resistance to spread within the head, also termed rachis resistance, which is assessed as the percentage of infected florets over time following the inoculation of a single floret (Schroeder and Christensen, 1963; Zhang et al., 2018). Quantitative trait loci (QTL), such as *Fhb1* and *Fhb2* that provide type II resistance, and *Fhb5* that confers type I resistance, derived from the Chinese spring wheat cultivated variety Sumai 3 are the major sources of FHB resistance, but only provide partial protection (Buerstmayr et al., 2009; Zhang et al., 2018). Genetic sources of complete FHB resistance have not yet been identified in wheat. Currently the most effective FHB management strategies integrate chemical fungicide treatment, agronomic practices that discourage the development of pathogen inoculum (e.g. crop

rotation), and the selection of moderately resistant wheat varieties (that have *Fhb* loci) (Dweba et al., 2017). Still, under favorable environmental conditions even this integrated approach frequently fails to consistently minimize disease and keep mycotoxin contamination below regulatory levels (Dweba et al., 2017).

Recent studies suggest that rising atmospheric CO_2 concentration also has the potential to compromise wheat resistance to FHB and associated DON contamination (Kane et al., 2013; Váry et al., 2015; Bencze et al., 2017). Transcriptomic analyses comparing winter wheat grown under ambient and elevated CO_2 conditions revealed that elevated CO_2 markedly supressed the expression of important plant defense response genes (Kane et al., 2013). Additionally, single-floret inoculations (evaluation of type II resistance) of winter wheat varieties with *Fusarium culmorum* usually resulted in higher grain DON content at elevated CO_2 than at ambient CO_2, even in the absence of visual disease differences (Bencze et al., 2017). However, with whole-head inoculations (evaluation of type I resistance), disease and DON content of grain grown at elevated CO_2 either did not change, decreased, or increased, depending on the host variety (Bencze et al., 2017). Furthermore, acclimation of *Fg* and spring wheat to elevated CO_2 resulted in greater disease development, and reduced effectiveness of innate plant defenses in a moderately resistant variety originating from Sumai 3 (Váry et al., 2015).

These findings amplify concerns that the occurrence of FHB and highly DON contaminated grain will rise under projected future climatic conditions. Rising CO_2, in particular, will be a global and consistent abiotic pressure that can influence wheat susceptibility to FHB and ultimately grain productivity and food safety. However, in order to develop more climate

resilient FHB resistant wheat varieties and agricultural management strategies, additional research is needed to understand the underlying processes involved, such as determining changes that occur in the wheat's defense response to *Fg* at elevated CO_2 leading to altered resistance.

Wheat resistance to FHB is dependent on a highly complex and integrated network of chemical defense metabolites that counteract *Fg* infection (Gauthier et al., 2015). Metabolomics, the high throughput analysis of metabolites in biological systems, have aided in the identification of many wheat resistance related metabolites, and metabolic biomarkers which can be used in breeding for enhanced resistance (Gunnaiah and Kushalappa, 2014; Gunnaiah et al. 2012; Hamzehzarghani, 2007; Cuperlovic-Culf et al., 2016; Dhokane et al., 2016). Metabolomics measurements can be performed on variety of samples from cell extracts and cell media or tissue extracts and body fluids, with preferred analytical methods currently being Nuclear Magnetic Resonance (NMR) spectroscopy or Mass spectrometry preceded by chromatography separation. Mass spectrometry provides information about larger number of compounds and is particularly appropriate for analysis of small samples and qualitative analysis. Metabolomics analysis in current work was performed for a large number of samples collected over time and NMR was chosen as a more appropriate method due to its high reproducibility, minimal sample preparation, possibility to identify compounds that are difficult to ionize or require derivatization and possibility for metabolite quantification over a wide dynamic range. Analysis of NMR data can be performed in an untargeted or qualitative sense, where all measured signals are analyzed and compared or in a targeted or quantitative sense where

accurate identification and quantification of defined set of metabolites is performed initially and these quantitative data is further analyzed (Bingol, 2018). In this study we have used both approaches where overall comparison of samples is performed in an untargeted sense and then quantitative metabolite data is used for more detailed analysis and biological interpretation.

In the present study, we evaluated the impact of elevated CO_2 on the metabolic response of spring wheat to *Fg* inoculation and assessed how changes in the defense response influenced susceptibility to FHB and DON contamination. In order to determine the potential underlying causes for changes in host resistance level, we used targeted and non-targeted metabolomics to compare the biochemical response of whole-head *Fg* inoculated wheat under ambient and elevated CO_2 conditions. To determine if elevated CO_2 impacted the response of wheat varieties containing *Fhb* loci differently, we evaluated the metabolic response of both a susceptible (Norm) and a moderately resistant (Alsen, which contains the *Fhb1* and *Fhb5* loci (Bai, 1996)) variety of wheat. Furthermore, we assessed for *Fg* isolate specific effects, and the potential influence of DON production on the host defense responses by using two distinct wild-type *Fg* isolates (9F1 and Gz3639), which have consistently produced DON and spread in previous disease assays, and a mutant form of Gz3639 (Gzt40), which lacks a functional biosynthetic (Tri5) gene and thereby is incapable of producing DON (Desjardins et al., 1996). Since wheat variety was a major contributor to metabolic differences, we also examined particular metabolic biomarkers for resistance that are not affected by CO_2 level.

Results

Preliminarily experiments determined that the published method of pathogen acclimation (Váry et al., 2015) by performing multiple consecutive subcultures at corresponding CO_2 concentrations results in virulence variability between strains that is not associated with CO_2 concentration. Recent reports similarly suggest that subculturing fungal isolates can result in altered virulence (Jirakkakul et al., 2018). Additionally, since our research objective was focused on the host responses, the *Fg* isolates were not acclimated to the different CO_2 concentrations, and inoculums were all treated identically prior to inoculations.

The effect of elevated CO_2 on wheat-*Fg* interactions following whole-head inoculation was dependent on the host variety as well as the infecting *Fg* strain (Figure 1). At 2xCO_2, Alsen inoculated with *Fg* strain 9F1 displayed significantly more disease symptoms at both 3 and 7 dpi, and accumulated 23% more *Fg* biomass (measured as relative *Fg* DNA to wheat DNA), and 38% more DON (Figure 1 A-C), than respective plants inoculated at 1xCO_2. In contrast, Norm grown at 2xCO_2 and inoculated with 9F1 displayed significantly less disease symptoms at 3 days post inoculation (dpi) (Figure 1A). However, at 7 dpi no significant difference in incidence of spikelet infection was detected. It is worth noting that while our scoring method indicated that diseased florets were approaching 100% at both CO_2 concentrations, at 7 days post whole-head inoculation many of these florets were only partially symptomatic. Nevertheless, the amount of *Fg* biomass in the tissue collected 7 dpi was 30% lower in Norm plants at 2xCO_2 in comparison to respective plants at 1xCO_2 (Figure 1A, B). Despite lower *Fg* biomass at 2xCO_2, the amount of DON that accumulated in Norm was not significantly affected by CO_2 concentration,

which suggests that the amount of DON produced per unit pathogen biomass was greater at $2xCO_2$. Whole-head inoculation with Gz3639 resulted in significantly reduced pathogen biomass at $2xCO_2$ in both Alsen and Norm; even though only Alsen appeared to have less disease at 7 dpi (Figure 1D, E). Despite the reduction in *Fg* biomass, DON contamination was not significantly affected, suggesting that at $2xCO_2$ Gz3639 produced more DON per unit pathogen biomass in both wheat varieties (Figure 1E, F). As expected, the mutant *Fg* strain Gzt40, which lacks a functional *Tri5* gene and thereby is incapable of producing DON, caused less disease overall (Figure 1G, H). No significant difference was visually observed between the Gzt40 inoculated plants at $2xCO_2$ in comparison to $1xCO_2$. However, on average the amount of Gzt40 biomass was reduced in plants grown at $2xCO_2$, although this reduction was only significant in susceptible variety Norm (Figure 1G, H).

To elucidate the underlying molecular processes involved in the observed differences in FHB and DON under $1xCO_2$ and $2xCO_2$ concentrations, we conducted metabolomic analyses of the host plant in response to different *Fg* treatments. 1D and 2D NMR measurements, including 1D proton, HSQC (heteronuclear single quantum coherence) and TOCSY (total correlated spectroscopy), were performed for hydrophilic metabolites in all samples. 1D proton spectra for all samples grouped by treatment and colored by sample type following spectral processing and alignments using the Icoshift method (Savorani, Tomasi, & Engelsen, 2010) are shown in Figure 2A. Signals from a mixture of water soluble compounds were detected with high signal quality and consistency across all measurements. Residual methanol solvent peaks were observed in the sample spectra (shown with yellow overlay in Figure 2) but were removed from the

analyses. No other impurities were detected. Minor differences in baseline and signal phasing were corrected as described in Material and Methods resulting in the high quality spectra used in analyses (Figure 2A).

Principal component analysis (PCA) of complete 1D spectra illustrated variances in the metabolic profiles across all samples based on complete metabolic profile in an untargeted, i.e. qualitative, sense (Figure 2B). In the PCA of all samples Principal component 2 (PC2) revealed major difference between metabolic profiles of Norm heads treated with DON producing *Fg* isolates (DON^+; 9F1 and Gz3639) and treatments lacking DON (DON^-; control and Gzt40). Although less pronounced, PC2 also showed separation between the metabolomes of DON^+ treated samples of Norm and Alsen. Furthermore, principal component 1 (PC1) illustrated some separation between the metabolomes of DON^- treatments and Alsen inoculated with DON^+ isolates. These results suggest that wheat variety and treatment were the most significant contributing factors to metabolic profile differences.

To further evaluate metabolic differences between wheat varieties and treatments, additional PCA was conducted on subgroups of samples. Separate PCA of Norm and Alsen wheat samples under different treatments (Figure 3A) revealed that in Norm the metabolic profiles of control and Gzt40 treated heads clustered, but distinctly separated from 9F1 and Gz3639 (DON^+) treated heads. However, the metabolic profiles of Alsen treated with Gzt40, noticeably separated from both the controls and the DON^+ fungal treatments. This would suggest that Alsen metabolically responds to *Fg* even in the absence of DON, and this response is different when the *Fg* strains produce DON. Differences between the metabolic responses of

202 Norm and Alsen became apparent when PCA was performed separately for each treatment of
203 Norm and Alsen wheat (Figure 3B). Greatest separation between Alsen and Norm
204 metabolomes was observed in Gz3639 and Gzt40 treated heads. However, separation for the
205 two varieties were illustrated by PC1 for Gz3639 and PC2 for Gzt40. The effect of CO_2 level was
206 difficult to discern in the presence of dominant source of variation (host variety), so a
207 supervised analysis was performed via O-PLS. This analysis determines combinations of
208 components in the spectral data that separate 1xCO_2 and 2xCO_2 samples for all treatments
209 (Figure 3C). Control and Gz3639 treated samples displayed the most distinct separation
210 between 1xCO_2 and 2xCO_2 as illustrated by PC1.

211 Targeted metabolites were used to also quantitatively analyze the data. Assignment and
212 determination of relative metabolite concentrations was performed as described in Materials
213 and Methods with the list of analyzed metabolites and their 1D spectra shown in
214 Supplementary Figure 1.

215 The resulting relative concentrations for the 49 identified metabolites following scaling
216 to a mean of zero and standard deviation of 1 across metabolites and samples are graphically
217 represented in a heat plot (Figure 4). This schematic (Figure 4) illustrates the variability
218 between metabolic profiles across wheat varieties, treatments, but also amongst biological
219 replicates. For example the concentration of glutamine in control Norm samples appears to be
220 more abundant in half of the samples but less abundant in the other half, at both CO_2
221 concentrations. It is worth noting that although the concentration of shikimate was relatively
222 low (also Supplementary Figure 3) and varied between samples, the average concentration in

223 Alsen was significantly higher than Norm in DON^+ *Fg* treatments and displayed a slight
224 reduction at $2xCO_2$.Comparison of PCA for spectral and quantitative metabolic data is shown in
225 Supplementary Figure 2. PCA of quantified metabolic data shows an overall agreement with the
226 PCA of spectra (Supplementary Figure 2) suggesting that major variances in the data have been
227 preserved in the quantification. Consistent with spectral analyses, metabolite concentrations
228 were primarily affected by wheat variety and treatment (as shown by hierarchical cluster
229 analysis in Supplementary Figure 4).

230 Significant differences between Alsen and Norm metabolite concentration for the
231 treatments were determined using Significance Analysis of Microarrays (SAM) (Tusher,
232 Tibshirani, & Chu, 2001). The metabolites with significant concentration differences between
233 Alsen and Norm for each treatment, independent of CO_2 concentration, were graphically
234 represented in a heat plot for each treatment (Figure 5). Significant differences in metabolite
235 concentrations between Norm and Alsen were found even without any *Fg* treatment (control).
236 Relative to Norm, control Alsen samples had higher concentrations of glutamate, L-(-)-
237 glutathione, phosphocholine, and L-alanine, and lower concentrations of beta-alanine,
238 succinate, trehalose, raffinose, oxoglutarate, methionine, leucine, asparagine and
239 phenylalanine (Figure 5). However, more metabolites displayed significant differences with *Fg*
240 inoculation. Based on the SAM, the metabolites which were significantly less abundant in Alsen
241 then Norm, regardless of treatment included: beta-alanine, succinic acid, oxoglutarate,
242 trehalose, raffinose, methionine and leucine (Figure 5, shown with blue dot). The
243 concentrations of asparagine and phenylalanine in control Alsen samples were lower than in

control Norm samples, but significantly higher in Alsen than Norm with *Fg* treatment, including Gzt40, suggesting that the induction of these metabolites was not DON dependent. Metabolic differences between Alsen and Norm treated with 9F1 and Gz3639, which both produce DON (DON^+), overlapped significantly and are indicated by red lines in Figure 5. Six of these metabolites also displayed differences with Gzt40 treatment (indicated with red circles in Figure 5). However, while the concentration of tryptophan was greater in DON^+ inoculated Alsen than respective Norm plants, the amount of tryptophan was lower in Gzt40 inoculated Alsen.

Metabolite markers that can distinguish between susceptible and resistant FHB wheat varieties are in high demand (Cuperlovic-Culf et al., 2016) with particular interest in the effect of rising CO_2 on the concentrations of these markers and their potential diagnostic accuracy with climate change. Therefore, features providing the highest classification power for Norm vs. Alsen wheat in control, mock-treated, samples were further selected using logistic regression and ANOVA analysis. According to the analysis, the metabolites with the highest classification power were: L-alanine, isoleucine, 3-hydroxybutarate and myoinositol (indicated with red X in Figure 5). The concentrations of these four metabolites also provide high classification accuracy between Alsen and Norm wheat regardless of atmospheric CO_2 level, as shown with PCA graph in Supplementary Figure 5. Also, Naïve Bayesian classifier shows high classification accuracy with obtained area under receiver operating curve (AUC) and the classification precision of 95.5% for these four markers. Although concentrations of these four markers varied at $2xCO_2$ in both Alsen and Norm (Figure 5 and Supplementary Figure 3), their relative concentration

remained different suggesting that the power of these resistance markers will be preserved even as CO_2 concentrations rise.

Features providing the highest classification accuracy for Norm and Alsen wheat in all samples, with all treatments and at both CO_2 levels according to Naïve Bayes analysis (AUC of 94.4%) are: sucrose, methionine, asparagine, oxoglutarate, tyrosine, phenylalanine, raffinose, L-alanine and succinate (not shown as separate figure). These metabolites have been selected as significantly different in individual SAM analysis for some or all treatments.

To identify the metabolic differences between $1xCO_2$ and $2xCO_2$ samples, we have used a logistic regression and ANOVA significance test followed by PCA of samples showing level of separation. Metabolites with the greatest significant differences between $1xCO_2$ and $2xCO_2$ with respect to treatments are shown in Figure 6.

An analysis of all samples, distinguished only by CO_2 concentration, revealed that on average malate, betaine, phosphocholine, oxoglutarate, succinate, glutamine and phenylalanine concentrations were higher in plants at $1xCO_2$, while uridine and sucrose concentrations tended to be higher in plants at $2xCO_2$ (Figure 6A). The major effect CO_2 level on these metabolites may reflect the changes that occur in primary metabolism at higher atmospheric CO_2.

As above, the data were further analyzed for each treatment independent of the others (Figure 6B). There was little overlap between the most significantly different metabolites of the treatments. However within the individual treatments, some of the same metabolites differed in both Norm and Alsen (shown with blue highlight in Figure 6B). Only the concentration of

cysteine was consistently different between the CO_2 concentrations in all the *Fg* treated Norm plants. Furthermore, the amount of cysteine was more abundant in Gzt40 inoculated Norm and Alsen plants at $2xCO_2$. Choline and myoinositol were significantly different at $1xCO_2$ in comparison to $2xCO_2$ in all *Fg* treated Alsen plants (shown with black X's in Figure 6B). However, the concentration of myoinositol in Alsen treated with Gz3639 or Gzt40 was greater in plants at $2xCO_2$ in comparison to $1xCO_2$, but not in 9F1 treated Alsen. Furthermore, the concentration of asparagine was different in $1xCO_2$ vs $2xCO_2$ Alsen plants treated with DON^+ *Fg* and control (indicated in Figure 6B with red X's), however the direction of the change was opposite in 9F1 and Gz3639 treatments. Additional analyses elucidating the major metabolic differences in *Fg* treated Alsen relative to the control treatment at both CO_2 levels are shown in Supplementary Figure 6 with Supplementary Figure 3 showing average concentrations for several metabolites of interest.

Discussion

To the best of our knowledge, this work represents the first report on differences in the metabolic profiles of *Fg* inoculated wheat at ambient and elevated CO_2. Our results demonstrate that the effects of elevated atmospheric CO_2 on FHB and DON contamination are dependent on both the *Fg* strain and the wheat variety. Furthermore, changes in host metabolites can partly explain the observed changes in FHB and DON levels. Previous studies observed variable effects of elevated CO_2 on head blight between wheat varieties, and have suggested that CO_2 has the potential to affect both the fungal pathogen and host plant (Kane et al., 2013; Váry et al., 2015; Bencze et al., 2017). Bencze et al. (2017), further demonstrated that

306 inoculation method, single floret vs whole-head (evaluating type I vs type II resistance
307 respectively), can produced variable results at elevated CO_2. However, our data provides
308 additional insight into the effects of elevated CO_2 on the metabolome of wheat varieties with
309 (Alsen) and without (Norm) *Fhb* loci in response to whole-head inoculation with two DON
310 producing (DON^+) *Fg* isolates and a mutant DON deficient (DON^-) *Fg* isolate.

311 Our results also indicate that visual disease severity and *Fg* biomass do not always
312 correspond with DON contamination levels (Figure 1). Climate can skew the classic disease
313 triangle and inlayed mycotoxin triangle in different ways (Medina et al. 2017). Our results are
314 consistent with other reports evaluating *Fusarium* diseases under abiotic stress conditions
315 (Paterson and Lima, 2010; Vaughan et al., 2014; Bencze et al., 2017). When pathogen
316 proliferation was constrained at $2xCO_2$, DON production per unit *Fg* biomass was higher (Figure
317 1B,C and D,F), leading to the observed reduction in pathogen biomass but no significant
318 difference in DON for Norm inoculated with 9F1, and both Norm and Alsen inoculated with
319 Gz3639 (Figure 1B,C and D,F). Furthermore, the increased resistance of Norm at $2xCO_2$ was
320 independent of DON production (Figure 1H), suggesting that $2xCO_2$ may compromise other
321 pathogen effectors, enhance host defenses, or a combination of both. Nevertheless, an
322 increase in DON production per unit *Fg* biomass is concerning. While the susceptible variety
323 Norm appears to have enhanced resistance to *Fg* colonization at $2xCO_2$, DON contamination
324 remained the same. Therefore, current mycotoxin food safety issues will persist. Additionally,
325 while current FHB control strategies and breeding efforts rely heavily on parent lines containing
326 *Fhb* loci for resistance, it is disturbing that these moderately resistant lines may become

significantly more susceptible to mycotoxin accumulation when infected by certain *Fg* strains at elevated CO_2 (Figure 1B,C).

The metabolic profiles of *Fg* inoculated Alsen and Norm were quite distinct. Multiple metabolites with significant concentration differences were identified between the varieties and treatments. All of the 49 quantified metabolites can be produced by *Fg* and wheat, thus without conducting separate analyses of *Fg* alone or carbon labelling experiments we can not be certain which organism is responsible for these metabolic changes during the interaction. Trehalose has been shown to play an important role in *Fg* virulence and mycotoxin production (Song et al., 2014), thus lower levels in Alsen are consistent with enhanced FHB resistance. On the other hand, asparagine has been described as a constitutive defense metabolite marker, and phenylalanine has been reported as a DON induced resistance metabolite in wheat (Paranidharan, 2008). However, asparagine and phenylalanine levels were higher in control Norm as compared to Alsen, but their concentrations were significantly higher in Alsen inoculated with 9F1, Gz3639 or Gzt40, suggesting that these metabolites would best be considered as inducible markers that are not always dependent on DON production. The production of asparagine may deprive the pathogen of a necessary nitrogen source (Seifi, et al. 2013) which is in agreement with increased asparagine concentration in Alsen plants treated with *Fg*. The lower concentration of succinate, oxoglutarate, methionine and leucine, together with the higher levels of phenylalanine and asparagine in *Fg* treated Alsen, suggests an increased flux in the shikimate pathway. Indeed, although quite variable and at relatively low concentration overall, the average concentration of shikimate was significantly higher in Alsen

in comparison to Norm for all treatments (Figure 4 and Supplementary Figure 3), which is consistent with previous reports on the metabolomes of other moderately resistant varieties including Sumai 3 (Cuperlovic-Culf et al., 2016). Phenylalanine is an end product of the shikimate pathway, and the starting substrate of the phenylpropanoid pathway; these pathways provide essential precursors for a wide range of important FHB resistance metabolites. For example, both salicylic acid, a key defense-related hormone, and flavonoids, which typically possess antioxidant activity, are phenylpropanoids (Gunnaiah and Kushalappa, 2014; Makandar et al., 2012). Chemical resistance mechanisms of wheat varieties containing the *Fhb* loci rely on induction of phenylpropanoids and thickening of cell walls that reduce pathogen advancement and synthesis of antifungal and antioxidant metabolites that reduce pathogen proliferation and DON production (Gunnaiah and Kushalappa, 2014). Therefore, the metabolic response of Alsen to *Fg* inoculation appears to be consistent with reports from other *Fhb* containing varieties. Additionally and perhaps most imperative, the metabolic pathways that contribute to the primary source of FHB resistance, appear to be upregulated in *Fg* inoculated Alsen relative to Norm at both CO_2 concentrations. Therefore, *Fhb*-containing varieties will likely remain more resistant to FHB than non *Fhb*-containing varieties even at elevated CO_2. This is consistent with our disease assessment results (Figure 1), and previously published data (Váry et al., 2015). Even in the case where the 9F1 biomass and DON concentration were significantly higher in Alsen at $2xCO_2$ in comparison to $1xCO_2$, these levels were still less than the amounts in corresponding Norm plants.

Metabolic differences were also found between 1xCO_2 and 2xCO_2 samples (Figure 3C and 6). Metabolic differences between control plants at the two CO_2 concentrations were expected given that elevated CO_2 can increases wheat photosynthesis and alter primary metabolism (Habash et al., 1995; Pal et al., 2005). A higher concentration of sucrose at elevated CO_2 is in agreement with previously observed increases in the expression of genes associated with sucrose synthesis (Fukayama et al., 2011; Gray & Brady, 2016). Several tricarboxylic acid (TCA) cycle intermediates including malate, oxoglutarate and succinate, were at lower concentrations at elevated CO_2, possibly due to increased flux through this pathway, another aspect which is supported by previous gene expression data (Fukayama et al., 2011; Gray & Brady, 2016).

Significant differences were also observed between the *Fg* treated samples, suggesting that *Fg* treatment was also a significant factor contributing to metabolic differences at the two CO_2 levels (Figure 3C and 6B). At 2xCO_2 not as much asparagine accumulated in Alsen treated with 9F1, which could explain the observed increase in susceptibility to 9F1 biomass and DON contamination. Only the concentration of glycerol significantly increased at 2xCO_2 in Alsen treated with 9F1 (Figure 6B). In barley, glycerol was identified as a putative resistance related metabolite (Bollina et al., 2011), but despite its induction here at 2xCO_2 in Alsen treated with 9F1 the plants were relatively more susceptible. Therefore, increased concentration of glycerol alone is not sufficient to enhance resistance. In Alsen treated with Gz3639 at 2xCO_2, only the concentration of phosphocholine was significantly reduced, while all other metabolites with significant differences, including asparagine and phenylalanine, were increased in

concentration (Supplementary Figure 3). Additionally, the concentration of asparagine was slightly reduced at 2xCO_2 in Alsen treated with Gzt40, indicating that this response in the host was not entirely dependent on DON and is therefore unlikely a response to changes in fungal mycotoxin production as 2xCO_2. Nevertheless, in moderately resistant wheat varieties carrying the *Fhb* loci, asparagine concentration may represent a useful biomarker for enhanced wheat susceptibility at elevated CO_2. It has been proposed that moderately resistant wheat varieties hinder DON production and fungal growth, by sequestering nitrogen in asparagine making it unavailable to the invading pathogen (Fagard et al., 2014; Gaufichon, et al. 2016). The difference between asparagine levels in Alsen compared to Norm supports this premise. However, in comparison to corresponding plants at 1xCO_2, the concentration of asparagine was lower in Alsen treated with 9F1 at 2xCO_2, but greater in Alsen treated with Gz3639 at 2xCO_2. This difference in asparagine is therefore dependent on the infecting *Fg* strain and not only an inherent trait of the host. It is possible that the aggressiveness of *Fg* strains on a moderately resistant host variety is determined by its ability to inhibit the host from sequestering nitrogen in asparagine, and elevated CO_2 interferes with this process in a strain specific manner leading to the observed strain dependent results.

Another important resistance metabolite that significantly differed between 9F1 and Gz3639 treated Alsen at 2xCO_2 was myoinositol (Figure 6). Although myoinositol is listed amongst the metabolites with the greatest significant concentration difference between 1xCO_2 and 2xCO_2 for all three *Fg* treatments, at 2xCO_2 the concentration of myoinositol was significantly reduced in Alsen treated with 9F1, while it was increased in Alsen treated with

Gz3639 or Gzt40. Myoinositol functions as a building block for a variety of molecules that are involved in signal transduction including regulation of plant hormone receptors, mediation of abiotic and biotic defense responses, and fungal pathogen recognition (Gillaspy, 2011). Furthermore, a myoinositol is a precursor for D-glucuronic acid, which is an essential component of cell wall biosynthesis, and ascorbic acid, which has strong antioxidant activity (Gauthier et al., 2015). Alsen treated with Gz3639 or Gzt40 displayed a similar induction in myoinositol, choline and acetate concentration at 2xCO_2. As Gzt40 is a mutant form of Gz3639, it cannot be excluded that these metabolic differences are a result of 2xCO_2 induced changes in the fungus, rather than the host plant or a combination of changes in both the fungus and the host plant. The induction of these metabolites was not observed in Norm inoculated with Gz3639 or Gzt40 at 2xCO_2, but the inherent genotypic differences between the two varieties does not allow for such comparisons. Therefore, the potential direct effects of elevated CO_2 on *Fg* effectors/ virulence factors other than DON require further investigation.

In Norm treated with either 9F1 or Gz3639 all significantly different metabolites were less abundant at 2xCO_2 which is perplexing considering that in both cases *Fg* biomass was reduced but DON levels were unaltered. These two *Fg* treatments share the reduction of betaine and cysteine (Figure 6). Betaine, a major component of wheat anthers and germ, has been shown to stimulate *Fg* growth (Strange et al., 1974), and cysteine has been implicated in DON resistance (Gardiner et al., 2010). Therefore, a reduction in the concentration of these two metabolites could potentially explain the observed results. However, Norm treated with Gzt40 at 2xCO_2 also displayed less fungal biomass, suggesting that the increase in resistance was

independent of DON production. There are no common metabolites between the three *Fg* treatments in Norm. Thus further experiments are needed to elucidate the underlying mechanisms involved in constraining *Fg* biomass in Norm at 2xCO_2.

Additional metabolic profiling that includes the quantification of metabolites derived from the phenylpropanoid pathway, which make up the largest (more than 50%) chemical group of potential resistance metabolites against DON producing Fusarium species (Gauthier et al., 2015), will likely provide additional insight into the underlying mechanism involved in CO_2 induced changes in wheat resistance to FHB. Although, we were able to make inferences based on changes in the concentration of essential precursors, these inferences/ hypotheses need to be empirically validated.

Our findings suggest that individual *Fg* strains can respond differently to elevated CO_2. Váry et al., (2015) previously demonstrated that pathogen virulence can be influenced by CO_2 concentration, but here we further show that this influence is strain dependent. Given this variability amongst strains, rising CO_2 concentration has the potential to further shape *Fg* population dynamics by giving an advantage to strains that have increased pathogenicity under conditions of elevated CO_2. Nevertheless, since the effects of elevated CO_2 are dependent on both the pathogen strain and the host variety, it is essential to evaluate multiple combinations of diverse strains and varieties when conducting such analyses.

Finally, our analysis has also identified several promising, constitutive, FHB resistance markers, L-alanine, isoleucine, 3-hydroxybutarate and myoinositol, which have significant concentration differences between susceptible Norm and moderately resistant Alsen spring

452 wheat at both ambient and elevated CO_2. Metabolomic analyses of other wheat varieties have
453 similarly identified L-alanine, 3-hydroxybutarate and myoinositol as wheat FHB resistance-
454 related metabolite markers (Hamzehzarghani, 2007; Gunnaiah, et al. 2012; Kushalappa &
455 Gunnaiah, 2013). However, 3-hydroxybutyrate was previously reported as a constitutive
456 resistance-related metabolite marker (Gunnaiah, et al. 2012; Hamzehzarghani, 2007). In our
457 analysis, 3-hydroxybutyrate was less abundant in control Alsen as compared to Norm, but the
458 concentration of 3- hydroxybutyrate was significantly higher in Alsen treated with *Fg*
459 (Supplementary Figure 6) suggesting that the constitutive concentration of this particular
460 metabolite may not reflect resistance level in all varieties. Furthermore, isoleucine has been
461 reported as a metabolite related to mechanisms of resistance in barley against *Fg* (Bollina et
462 al., 2011; https://bioinfo.nrc.ca/mwfd/index.php). Nevertheless, the metabolic panel identified
463 here is unique in that it provides breeders with markers that will reliably predict resistance or
464 susceptibility, even as atmospheric CO_2 levels rise.
465

466 **Material and Methods**

467 **Experimental Design**

468 To evaluate the effect of elevated atmospheric CO_2 concentration on the metabolomic
469 response of wheat following *Fg* inoculation, we conducted FHB assays in growth chambers
470 programmed to ambient CO_2 (400 ppm, $1xCO_2$) and elevated CO_2 (800 ppm, $2xCO_2$). Second-
471 generation $1xCO_2$ and $2xCO_2$ acclimated (Váry et al., 2015) hard red spring wheat varieties
472 Norm and Alsen were used for all the experiments. Norm (pedigree = MN73167/MN 81070,

473 released by the Minnesota Agricultural Experiment Station and the U.S. Department of
474 Agriculture-Agricultural Research Service in 1992) is highly susceptible to head blight, while
475 Alsen (pedigree = ND 674//ND 2710/ND 688, released by the North Dakota Agricultural
476 Experiment Station in 2000), is derived from the resistant Sumai 3, and contains the *Fhb1* and
477 *Fhb5* loci (Bai, 1996). Two wild-type 15-acetyldeoxynivalenol (15-ADON) producing strains, 9F1
478 (isolated from the Netherlands; (McCormick et al., 2010)) and Gz3639 (isolated from Kansas,
479 US; (Desjardins et al., 1996)), as well as a trichothecene-nonproducing *tri5* deletion mutant
480 (Gzt40) of Gz3639 (Desjardins et al., 1996), were used. Whole-head inoculations were
481 conducted to test the combined resistance to the penetration and spread of the pathogen by
482 dipping the entire flowering wheat head in 50 mL of inoculum and then evaluating initial
483 disease symptoms at 3 days post infect and spread at 7 days post infection (type I + II
484 resistance). As a negative control, heads were mock-inoculated with sterile 0.04% Tween
485 solution. At each CO_2 concentration, 30 heads from at least 6 independent pots were
486 inoculated with one of the three *Fg* strains or the control 0.04% Tween solution. Following the
487 disease assays, three heads were combined into one tube as a single biological pool (resulting
488 in n=10 per treatment). Due to growth chamber space limitations and differences in flowering
489 time, experiments with Norm and Alsen were conducted separately.

490 **Wheat growth**

491 Five seeds were germinated in each 20 cm × 15 cm plastic pot filled with approximately
492 4 L of SunGrow Horticulture potting mix (Agawam, Massachusetts). Plants were grown in two
493 separate climate controlled growth chambers both programmed at 25°C day/23°C night, 550

494 µmol m^{-2} sec^{-1} photosynthetic photon flux density with a 14 h photoperiod, with 50–60%
495 relative humidity. The only difference in growing conditions was that one chamber was set at
496 400 ppm CO_2 ($1xCO_2$) and the other at 800 ppm CO_2 ($2xCO_2$). Plants were watered daily and
497 received bi-weekly nutrient supplement with soluble Peters 20-20-20 (The Scotts Company,
498 Marysville, OH, USA) until anthesis, at which point the flowering heads were inoculated.

499 ***Fg* inoculation and disease assessment**

500 Inoculum was prepared by recovering isolates from glycerol stocks, allowing them to
501 grow for 7 days on V8 plates, and then transferring an agar plug to 100 mL of mung bean broth.
502 Cultures were then grown at 28°C for 48 h at 200 rpm. The conidial suspension of each strain
503 was spun down and re-suspended in 0.04% Tween 20 (Fisher Scientific) solution at a
504 concentration of 10^5 microconidia mL^{-1}, based on cell counts obtained using a Scepter™
505 automated cell counter (Millipore, Billerica, MA, USA). Fresh inoculum was prepared on the day
506 of each experiment.

507 To minimize metabolic differences due to circadian rhythm, all experiment inoculations
508 were performed between 1:00-2:00 pm. Inoculated heads were covered with plastic bags to
509 ensure high humidity during the early stages of pathogenesis. Three days post inoculation (dpi)
510 the bags were removed and the number of visibly infected florets were scored. The heads were
511 again scored at 7 dpi, and then collected, frozen in liquid nitrogen, and kept at -80°C until
512 processing. All collections were done between 1:00-2:00 PM. Collected tissues were lyophilized
513 in a VirTis Lyophilizer (Model 24DX48GPFD 25LXL70, SP Scientific, Warminster, PA, USA) and
514 then pulverized using a SPEXsamplePrep Geno/Grinder 2010 (Metuchen, NJ, USA). Samples

were separated into 3 aliquots for DNA quantification of pathogen/plant biomass, mycotoxin quantification, and metabolite analyses.

Percent disease was calculated by dividing the number of visually symptomatic florets by the total number of florets on the head. Florets displaying any sign (even if minor) of premature beaching or spots of necrosis were deemed symptomatic. Student's t-tests were then performed to compare the average percentage of disease on plants grown at 1xCO_2 with those at 2xCO_2. Comparisons for Alsen and Norm varieties were conducted independently.

Estimation of pathogen/plant biomass

In order to assess the amount of fungal biomass in the inoculated tissues, the ratio of *Fg* DNA to wheat DNA was estimated using quantitative PCR (qPCR) (Vaughan et al., 2014). Genomic DNA was extracted from 80 mg of tissue ground using the ZR Fungal/Bacterial DNA MiniPrep and the Genomic DNA Clean and Concentrate kits (ZYMO Research, Boston, MA, USA) following the manufacturer's protocol. The quantity of 9F1 DNA was estimated using gene-specific primers for *Tri5* (forward TCTATGGCCCAAGGACCTGT and reverse ACGCTCATCGTCGAATTCCT; efficiency = 116, R^2=0.996) and the quantity of Gz3639 and Gzt40 was estimated using gene-specific primers for *Tri6* (forward TAACCACATCGTCGGGACTG and reverse GCCGACTTCTTGCAGGTCTT; efficiency = 116, R^2=0.996). The quantity of *Triticum aestivum* DNA was estimated using primers for *PR1* (forward CGTCTTCATCACCTGCAACTA and reverse CAAACATAAACACACGCACGTA; efficiency = 115; R^2=0.997). For DNA quantifications, a ten-fold dilution series spanning 6-logs from 50 ng of pure fungal or plant DNA was used to generate standard curves by plotting the Cq values obtained by qPCR against the log of DNA

concentration. Statistical differences between the *Fg*/wheat DNA biomass at 1xCO_2 and 2xCO_2 were determined by conducting pair-wise Student's t-tests.

Mycotoxin analyses

Mycotoxins were extracted from 0.5 g of pulverized tissue from the whole head with 10 mL extraction solvent (acetonitrile-water, 86:14 vol/vol) in a 50 mL polypropylene screw-cap centrifuge tube with shaking for 15 min. After centrifugation, a portion of each extract was purified by forcing 5 mL extract through a MycoSep 225 Trich cartridge (Romer Labs, Union, Missouri). A 2 mL aliquot of the purified extract was then transferred to a 1 dram vial and dried under a nitrogen stream. Trimethylsilyl (TMS) derivatives were prepared by adding 100 µL of a 100:1 freshly prepared mixture of N-trimethylsilylimadazole/trimethylchlorosilane (TMSI/TMCS) (Sigma-Aldrich, St. Louis, MO, USA) to the dried extract. After 30 min, 900 µL of isooctane were added to the reaction mixture followed by 1 mL water. The mixture was mixed gently until the organic (top) layer became translucent. The organic layer was then transferred to 2 mL autosampler vials for GC-MS analysis. TMS derivatives of purified DON (0.3125 µg to 80 µg) were also prepared to construct a standard curve for quantification. Significant differences between the amount of DON in Alsen or Norm at 1xCO_2 and 2xCO_2 were evaluated using pair-wise Student's t-test.

GC-MS analyses were performed on an Agilent 7890 gas chromatograph fitted with a HP-5MS column (30 m, 0.25 mm, 0.25 µm) and a 5977 mass detector. The injection temperature was kept at 250°C and the column flow rate was 1 mL min^{-1}. A temperature program was used with initial column temperature of 150°C for 1 min, and then increased to

280°C at 30°C min^{-1} and held for 3.5 min. Selective ion monitoring (SIM) was applied to detect the characteristic ions of triTMS-DON with fragment ion (m/z value) of 235.1 as the quantifier ion and 259.1, 295.1, 392.2, 422.2, and 512.2 as qualifier ions.

Metabolite extraction for NMR analysis.

Hydrophilic metabolites were extracted from approximately 100 mg (precise amount for each sample was recorded) of tissue with 1 mL of methanol:water solution (40:60 v/v) by homogenizing the sample for 30 sec at 6000 rpm using a Precellys 24 homogenizer (Bertin Technologies, Atkinson, NH, USA), followed by centrifugation at 3500 g for 20 min, and then collecting the supernatant into a 15 mL tube. The extraction process was repeated and the supernatants from both extractions were combined. The tubes where covered with Breath-Easier film (Diversified Biotech), frozen by placing the bottom of the tube in liquid nitrogen, and then lyophilized for 24-48 h. The dry samples were covered and then stored at -80°C. For NMR analysis the samples were re-suspended in 700 µL of deuterated phosphate buffer (0.0912 g monobasic potassium phosphate in 10 mL deuterium oxide was mixed with 0.1167 g dibasic potassium phosphate in 10 mL deuterium oxide to create a 0.067 M phosphate solution, to which 20 mg sodium azide and 20 mg deuterated sodium trimethylsilylpropionate (TSP) were added), vortexed, and transferred to NMR sample tubes.

NMR experimentation, data processing and quantification

All ^{1}H NMR measurements were performed on a Bruker 500 MHz spectrometer at 298 K. 1D ^{1}H (proton) NMR were measured for all samples using 1D ^{1}H with water suppression sequence. 2D TOCSY (Total Correlated Spectroscopy) and HSQC (heteronuclear single quantum

coherence) spectra were used for metabolite identification. All 1D and 2D spectra were processed using MestReNova 9.1.0 software (Mestrelab Research Solutions). Preprocessing for 1D spectra included: exponential apodization (exp 1); global phase correction; and normalization using the reference peak. Spectral regions from 0.5–9.5 ppm were included in the normalization and analysis. 2D spectra were processed using standard procedure recommended in the MestReNova documentation.

Metabolite assignment was performed using 1D ^{1}H, HSQC and TOCSY data. Assignment of peaks in the TOCSY spectra was performed using Madison Metabolomics Consortium Database and tools (Markley et al., 2007). Assignment of individual peaks was performed using searches provided in metabolomics databases HMDB (Wishart et al., 2013) and BMRB (Markley et al., 2007) as well as NMR spectral peaks search tool MetaboHunter (Tulpan et al. 2011) and literature assignments for metabolites previously observed in related samples. A total of 49 metabolites were included in the analyses, comprising molecules that were present in both TOCSY and HSQC spectra. Spectra for metabolites that were used in quantification of 1D ^{1}H spectra were obtained from the Human Metabolomics Database (www.hmdb.ca) or Biological Magnetic Resonance Databank (www.bmrb.wisc.edu) and processed using MestReNova 9.1.0 software. Spectral preprocessing for standards spectra included: exponential apodization (exp 1); global phase correction; and normalization using the total spectral area. Spectral regions from 0.5–9.5 ppm were included in the normalization and analysis. Prior to quantification analysis, the standard spectra were aligned to the reference peak (trimethylsilylpropionate) using peak alignment by fast Fourier transform cross-correlation (Wong, Durante, & Cartwright,

599 2005). The list of analyzed metabolites and their 1D spectra used for the determination of
600 relative concentrations in the sample spectra are shown in Supplementary Figure 1. The set of
601 quantified metabolites can be divided into carbohydrate pathway metabolites, amino acids and
602 derivatives, organic acids, and others. Metabolites from these chemical groups have previously
603 been linked to FHB resistance, and also provide insight in to potential fluxes in the biosynthetic
604 pathways other chemical groups involved in host resistance (Gauthier et al., 2015), because
605 many of the metabolites from the groups analyzed serve as precursors for others which have
606 not been directly evaluated in this study.

607 An automated method for quantification using multivariable linear regression that finds
608 the best fit of spectra for individual metabolites from database to the measured 1D sample
609 spectra was developed previously (Cuperlovic-Culf, Ferguson, Culf, Morin, & Touaibia, 2012)
610 and utilized in this study to determine relative metabolite concentrations. The partial least
611 square regression analysis result was used as the starting point and the model was constrained
612 to concentrations greater than or equal to zero. The deconvolution of spectra of mixtures, such
613 as in metabolomics, with many strongly overlapping lines, possibly with an unknown number of
614 lines and atomic groups, each with a different line width is extremely difficult and thus it is
615 important to determine an optimal solver for this problem. The best result, *i.e.* the model with
616 a minimal error was obtained with Levenberg-Marquardt curve fitting and this method was
617 used for quantification of metabolic data used in further analysis. Multivariate linear regression
618 analysis was performed using lsqcurvefit running under Matlab. Metabolite concentrations
619 across samples were determined using the same standard spectra that were normalized to the

total intensity equal to one and sample spectra normalized to the same reference concentration. The resulting concentrations therefore provide relative metabolite measures in different samples using the same standard scale that allows comparison between samples without having to determine absolute metabolite concentrations.

Data analysis

Pre-processing including data organization, removal of undesired areas, normalization, as well as data presentation was performed with Matlab vR2010 and vR2017a (Mathworks). Minor adjustments in peak positions (alignment) between different samples were performed using Icoshift (Savorani, Tomasi, & Engelsen, 2010). Principal component analysis (PCA) was performed in Matlab using routine ppca for probabilistic principal component analysis (Tipping, 1999) was performed on sample spectra as well as relative metabolite concentration data. Supervised classification analysis method Orthogonal projections to latent structures (O-PLS) running in Matlab was used to separate spectral data for the two CO_2 conditions. Selection of metabolic panels with statistically significant difference between groups was done using the Significance Analysis for Microarrays (SAM) method (Tusher, Tibshirani, & Chu, 2001) as provided in TMeV selecting panels with 0 false significant genes and Δ (delta) value of over 1 representing distance from the expected line based on the permutation analysis performed in SAM. Machine learning methods running under Matlab and Orange, a component based data mining software running under Anaconda Python Data Science Platform (https://anaconda.org/; https://orange.biolab.si/) were used for feature selection in different CO_2 concentrations. Specifically, feature selection was done using Logistic Ridge Regression

641 performing L2 regularization as well as ANOVA ranking as presented in Orange giving the same
642 set of significant metabolites.

643 **Acknowledgments**

644 Thanks to our exceptional technical staff Stephanie Folmar and Christine J. Hodges. Disclaimer: Mention
645 of trade names or commercial products in this publication is solely for the purpose of providing specific
646 information and does not imply recommendation or endorsement by the U.S. Department of
647 Agriculture. USDA is an equal opportunity provider and employer.

648

References

Desjardins, A. E., Proctor, R. H., Bai, G. H., McCormick, S. P., Shaner, G., Buechley, G., Hohn, T. M., 1996. Reduced virulence of trichothecene-nonproducing mutants of *Gibberella zeae* in wheat field tests. Mol. Plant-Microbe Interact. 9: 775-781

Bai, G.-H., Desjardins, A., Plattner, R. 2002. Deoxynivalenol-nonproducing *Fusarium graminearum* causes initial infection, but does not cause disease spread in wheat spikes. Mycopathologia 153: 91-98.

Barton B., and Clark S. 2014. Water and Climate Risks Facing U.S. Corn Production: How Companies and Investors Can Cultivate Sustainability. A Ceres Report. Boston, MABebber, D. P. 2015. Range-expanding pests and pathogens in a warming world. Annu. Rev. Phytopathol. 53: 335-356.

Bebber, D. P., Gurr, S. J. 2015. Crop-destroying fungal and oomycete pathogens challenge food security. Fungal Genet. Biol. 74: 62-64.

Bencze, S., Puskas, K., Vida, G., Karsai, I., Balla, K., Komaromi, J., Veisz, O., 2017. Rising atmospheric CO_2 concentration may imply higher risk of Fusarium mycotoxin contamination of wheat grains. Mycotoxin Res. 33: 229-236.

Bingo, L. 2018. Recent Advances in Targeted and Untargeted Metabolomics by NMR and MS/NMR Methods. High Throughput 7: 9.

Bollina, V., Kushalappa, A.C., Choo, T.M., Dion, Y., Rioux, S. 2011. Identification of metabolites related to mechanisms of resistance in barley against *Fusarium graminearum*, based on mass spectrometry. Plant Mol. Biol. 77: 355.

Buerstmayr, H., Ban, T., Anderson, J. A. 2009. QTL mapping and marker-assisted selection for Fusarium head blight resistance in wheat: a review. Plant Breeding. 128: 1-26.

Chakraborty, S., Newton, A. C. 2011. Climate change, plant diseases and food security: an overview. Plant Pathol. 60: 2-14.

Cuperlovic-Culf, M. Ferguson, Culf, A., Morin, P., Touaibia, M. 2012. 1H NMR metabolomics analysis of glioblastoma subtypes: correlation between metabolomics and gene expression characteristics. J. Biol. Chem. 287: 20164–75.

Cuperlovic-Culf, M., Wang, L., Forseille, L., Boyle, K., Merkley, N., Burton, I., Fobert, P. R. 2016. Metabolic Biomarker Panels of Response to Fusarium Head Blight Infection in Different Wheat Varieties. PLoS ONE. 11: e0153642.

Dhokane, D., Karre, S., Kushalappa, A. C., McCartney, C. 2016. Integrated Metabolo-Transcriptomics Reveals Fusarium Head Blight Candidate Resistance Genes in Wheat QTL-Fhb2. PLoS ONE. 11: e0155851.

Dweba, C., Figlan, S., Shimelis, H., Motaung, T., Sydenham, S., Mwadzingeni, L., Tsilo, T.J. 2017. Fusarium head blight of wheat: Pathogenesis and control strategies. Crop Prot. 91:114-122.

685 Edwards, S. G. 2004 Influence of agricultural practices on fusarium infection of cereals and
686 subsequent contamination of grain by trichothecene mycotoxins. Toxicol. Lett. 153: 29-35.

687 Fagard, M., Launay, A., Clément, G., Courtial, J., Dellagi, A., Farjad, M., … Masclaux-Daubresse,
688 C. 2014. Nitrogen metabolism meets phytopathology. J. Exp. Bot. 65(19): 5643–5656.

689 Fisher, M. C., Henk, D. a, Briggs, C. J., Brownstein, J. S., Madoff, L. C., McCraw, S. L., & Gurr, S. J.
690 2012 Emerging fungal threats to animal, plant and ecosystem health. Nature. 484: 186–94.

691 Fukayama, H., Sugino, M., Fukuda, T., Masumoto, C., Taniguchi, Y., Okada, M., Miyao, M. 2011.
692 Gene expression profiling of rice grown in free air CO_2 enrichment (FACE) and elevated soil
693 temperature. Field Crops Res. 121(1): 195–199.

694 Gardiner, S. A., Boddu, J., Berthiller, F., Hametner, C., Stupar, R. M., Adam, G., Muehlbauer, G. J.
695 2010. Transcriptome analysis of the barley-deoxynivalenol interaction: evidence for a role of
696 glutathione in deoxynivalenol detoxification. Mol. Plant-Microbe Interact. 23: 962-976.

697 Gaufichon, L., Rothstein, S. J., & Suzuki, A. 2016. Asparagine metabolic pathways in Arabidopsis.
698 Plant and Cell Physiol. 57(4): 675–689.

699 Gauthier, L., Atanasova-Penichon, V., Chereau, S., Richard-Forget, F. 2015. Metabolomics to
700 decipher the chemical defense of cereals against *Fusarium graminearum* and deoxynivalenol
701 accumulation. Int. J. Mol. Sci. 16: 24839-24872.

702 Gillaspy G. 2011. The cellular language of myo-inositol signaling. New Phytol. 192: 823-839.

703 Gray, S. B., & Brady, S. M. 2016. Plant developmental responses to climate change. Dev. Biol.
704 419(1): 64–77.

705 Gunnaiah, R., Kushalappa, A. C. 2014. Metabolomics deciphers the host resistance mechanisms
706 in wheat cultivar Sumai-3, against trichothecene producing and non-producing isolates of
707 *Fusarium graminearum*. Plant Physiol. Bioch. 83: 40-50.

708 Gunnaiah, R., Kushalappa, A. C., Duggavathi, R., Fox, S., & Somers, D. J. 2012. Integrated
709 metabolo-proteomic approach to decipher the mechanisms by which wheat qtl (Fhb1)
710 contributes to resistance against *Fusarium graminearum*. PLoS ONE. 7(7).

711 Habash, D. Z., Paul, M. J., Parry, M. A. J., Keys, A. J., Lawlor, D. W. 1995. Increased capacity for
712 photosynthesis in wheat grown at elevated CO_2: the relationship between electron transport
713 and carbon metabolism. Planta 197: 482-489.

714 Hamzehzarghani, H. 2007. Metabolic profiling and multivariate analysis to phenotype cultivars
715 of wheat varying in resistance to fusarium head blight. Ph.D. Thesis.

716 Hogy, P., Wieser, H., Kohler, P., Schwadorf, K., Breuer, J., Franzaring, J., Muntifering, R.,
717 Fangmeier, A. 2009. Effects of elevated CO2 on grain yield and quality of wheat: results from a
718 3-year free-air CO2 enrichment experiment. Plant Biol. 11:60-69.

719 Kane, K., Dahal, K. P., Badawi, M. A., Houde, M., Huner, N. P., Sarhan, F. 2013. Long-term
720 growth under elevated CO_2 suppresses biotic stress genes in non-acclimated, but not cold-
721 acclimated winter wheat. Plant Cell Physiol. 54: 1751-1768.

722 Kushalappa, A. C., & Gunnaiah, R., 2013. Metabolo-proteomics to discover plant biotic stress
723 resistance genes. Trends Plant Sci. 18(9): 522–531.

724 Madgwick, J., West, J., White, R., Semenov, M., Townsend, J., Turner, J., Fitt, B. L. 2011. Impacts
725 of climate change on wheat anthesis and fusarium ear blight in the UK. Eur. J. Plant Pathol. 130:
726 117-131.

727 Makandar, R., Nalam, V. J., Lee, H., Trick, H. N., Dong, Y., Shah, J., 2012. Salicylic acid regulates
728 basal resistance to Fusarium head blight in wheat. Mol. Plant-Microbe Interact. 25: 431-439.

729 Markley, J. L., Anderson, M. E., Cui, Q., Eghbalnia, H. R., Lewis, I. a, Hegeman, A. D., Zolnai, Z.
730 2007. New bioinformatics resources for metabolomics. Pacific Symposium on Biocomputing.
731 168: 157–68.

732 Medina A., Akbar A., Baazeem A., Rodriguez A., Magan N. 2017. Climate change, food security
733 and mycotoxins: Do we know enough? Fungal Biol. Rev. 31 (3): 143-154.

734 McCormick, S. P., Alexander, N. J., Harris, L. J. 2010. CLM1 of *Fusarium graminearum* encodes a
735 longiborneol synthase required for culmorin production. Appl. Environ. Microbiol. 76: 136-141.

736 Mesterhazy, A., Bartok, T., Mirocha, C., Komoroczy, R. 1999. Nature of wheat resistance to
737 Fusarium head blight and the role of deoxynivalenol for breeding. Plant Breeding 118: 97-110.

738 NOAA, 2017 https://esrl.noaa.gov/gmd/ccgg/trends/global.html#global

739 Pal, M., Rao, L. S., Jain, V., Srivastava, A. C., Pandey, R., Raj, A., Singh, K. P., 2005. Effects of
740 elevated CO_2 and nitrogen on wheat growth and photosynthesis. Biol. Plant. 49: 467-470.

741 Paranidharan V., Abu-Nada Y., Hamzehzarghani H., Kushalappa A. C., Mamer O., Dion Y., Rioux
742 S., Comeau A., Choiniere L. 2008. Resistance-related metabolites in wheat against *Fusarium*
743 *graminearum* and the virulence factor deoxynivalenol (DON). Botany. 86(10):1168–1179.

744 Paterson, R. R. M., Lima, N. 2010. How will climate change affect mycotoxins in food? Food Res.
745 Int. 43: 1902-1914.

746 Pestka, J. 2010. Toxicological mechanisms and potential health effects of deoxynivalenol and
747 nivalenol. World Mycotoxin J. 3: 323-347.

748 Savorani, F., Tomasi, G., Engelsen, S. B. 2010. icoshift: A versatile tool for the rapid alignment of
749 1D NMR spectra. J. Magn Reson. 202(2): 190–202.

750 Schroeder, H. W., Christensen, J. J.,1963. Factors affecting resistance of wheat to scab caused
751 by *Gibberella zeae*. Phytopathology. 53: 831-838.

752 Seifi, H. S., Van Bockhaven, J., Angenon, G., & Höfte, M. 2013. Glutamate metabolism in plant
753 disease and defense: friend or foe? Mol. Plant-Microbe Interact. 26(5): 475–85.

Song, Xiu-Shi, Li, He-Ping, Zhang, Jing-Bo, Song, Bo, Huang, Tao, Du, Xiao-Min, Gong, An-Dong, Liu, Yi-Ke, Feng, Yan-Ni, Agboola, Rebecca S., Liao, Yu-Cai. 2014. Trehalose 6-phosphate phosphatase is required for development, virulence and mycotoxin biosynthesis apart from trehalose biosynthesis in *Fusarium graminearum*. Fungal Genet. Biol. 63:24–41.

Stocker, T.F., Qin D, Plattner G-K, Tignor M, Allen SK, Boschung J,. 2013. Climate Change 2013: The Physical Science Basis. Contribution of Working Group I to the Fifth Assessment Report of the Intergovernmental Panel on Climate Change Cambridge, United Kingdom and New York, NY, USA.

Strange, R. N., Majer, J. R., Smith, H. 1974. The isolation and identification of choline and betaine as the two major components in anthers and wheat germ that stimulate *Fusarium graminearum* in vitro. Physiol. Plant Path. 4: 277-290.

Tipping, M. E., and C. M. Bishop. 1999. Probabilistic Principal Component Analysis. J. Royal Stat. Soc. 61(3):611–622.

Tulpan, D., Léger, S., Belliveau, L., Culf, A., & Cuperlović-Culf, M. 2011 MetaboHunter: an automatic approach for identification of metabolites from 1H-NMR spectra of complex mixtures. BMC Bioinf. 12: 400.

Tusher, V. G., Tibshirani, R., & Chu, G., 2001. Significance analysis of microarrays applied to the ionizing radiation response. Proc. Natl. Acad. Sci. U.S.A. 98(9): 5116–21.

Váry, Z., Mullins, E., McElwain, J. C., Doohan, F. M. 2015. The severity of wheat diseases increases when plants and pathogens are acclimatized to elevated carbon dioxide. Glob. Change Biol. 21:2661-2669.

Vaughan, M. M., Backhouse, D., Del Ponte, E. M. 2016. Climate change impacts on the ecology of *Fusarium graminearum* species complex and susceptibility of wheat to Fusarium head blight: A review. World Mycotoxin J. 9: 685-700.

Vaughan, M. M., Huffaker, A., Schmelz, E. A., Dafoe, N. J., Christensen, S., Sims, J., Martins, V. F., Swerbilow, J. A. Y., Romero, M., Alborn, H. T., Allen, L. H., Teal, P. E. A. 2014. Effects of elevated [CO_2] on maize defense against mycotoxigenic *Fusarium verticillioides*. Plant, Cell & Environ. 37: 2691-2706.

Wishart, D. S., Jewison, T., Guo, A. C., Wilson, M., Knox, C., Liu, Y., Scalbert, A. 2013, HMDB 3.0-The Human Metabolome Database in 2013. Nucleic Acids Res. 41: 801–807.

Wong, J.W.H., Durante, C., Cartwright, H.M. 2005. Application of fast fourier transform cross-correlation for the alignment of large chromatographic and spectral datasets. Anal. Chem. 77(17): 5655–5661.

Wu, F., Groopman, J. D., Pestka, J. J. 2014. Public health impacts of foodborne mycotoxins. Annu. Rev. Food Sci. T. 5: 351-372.

Zhang, W., Francis, T., Gao, P., Boyle, K., Jiang, F., Eudes, F., Cuthbert, R., Sharpe, A., Fobert, P. R. 2018. Genetic characterization of type II Fusarium head blight resistance derived from

transgressive segregation in a cross between Eastern and Western Canadian spring wheat. Mol. Breed. 38: 13.

Zhang, X., Halder, J., White, R. P., Hughes, D. J., Ye, Z., Wang, C., Xu, R., Gan, B., Fitt, B. D. L. 2014. Climate change increases risk of fusarium ear blight on wheat in central China. Ann. Appl. Biol. 164: 384-395.

Figure Legend

Figure 1. Effect of elevated CO_2 on FHB development in susceptible (Norm) and moderately resistant (Alsen) wheat hosts caused by two wild-type *Fg* strains (9F1 and Gz3639) and a mutant strain (Gzt40) disrupted in deoxynivalenol (DON) production. Average percent symptomatic spikelets per head observed on day 3 and day 7 post whole-head inoculation with 9F1, Gz3639, or Gzt40 on Alsen or Norm grown at 1xCO_2 (400 ppm) and 2xCO_2 (800 ppm) (A, D, G). Average pathogen biomass measured as *Fg* DNA (9F1, Gz3639 or Gzt40) relative to wheat DNA (Alsen or Norm) at day 7 post inoculation under 1xCO_2 or 2xCO_2 (B, E, H). Average DON contamination in Alsen and Norm wheat heads 7 days post inoculation with 9F1 or Gz3639 under 1xCO_2 or 2xCO_2 (C and F). Bars indicate standard error of the mean (SEM) and colored asterisks designate significant differences (Means from Alsen and Norm were analyzed separately using t-test's to compare differences between 1xCO_2 and 2xCO_2, $P < 0.05$).

Figure 2. A. Average 1D ^{1}H spectra grouped by treatment. Blue lines represent spectra for Norm and red lines represent spectra for Alsen. Yellow overlay highlights the methanol peak. B. PCA of spectra for all samples labelled by wheat variety (outline color), *Fg* treatment type (fill color), and 800 ppm CO_2 (2xCO_2) level marked with an "x". Metabolite profiles clustered into three distinct groups indicated by different color circles: Blue circle surrounds Norm inoculated with DON producing (DON^+) *Fg* strains (9F1 and Gz3639) samples; red circle groups Alsen inoculated with DON producing (DON^+) *Fg* strains (9F1 and Gz3639); green circle clusters the mock-inoculated (Control) and Gzt40 inoculated samples from both Norm and Alsen. Percentage of total variation in the spectral data that is accounted for in principal components PC1 and PC2 is provided.

Figure 3. Analysis of 1D ^{1}H NMR spectra. A. PCA of all, complete 1D ^{1}H NMR spectra comparing the metabolic profiles of Norm (top) and Alsen (bottom) wheat in response to treatments (Control, 9F1, Gz3639 and Gzt40) at both CO_2 concentrations. Percentage of total variation in the spectral data that is accounted for in principal components PC1 and PC2 is provided.; B. PCA of 1D ^{1}H NMR spectra showing differences between the metabolic responses of Norm and Alsen to different treatments. Percentage of total variation in the spectral data that is accounted for in principal components PC1 and PC2 is provided for each plot. C. O-PLS analysis illustrating the effect of CO_2 level on metabolic responses for each treatment.

Figure 4. Heat map of targeted metabolite concentrations relative to the reference trimethylsilylpropionate peak and scaled to calculated mean of 0 and standard deviation of 1

across all samples and metabolites with red indicating samples with significantly higher metabolite concentration than the overall metabolite mean and green indicating lower metabolite concentration than mean concentration. Metabolites are ordered based on their concentration similarities across all samples determined with hierarchical clustering. Relative concentrations prior to scaling are shown in Supplementary Figure 3 and the hierarchical clustering across samples and metabolites is presented in Supplementary Figure 4.

Figure 5. Metabolites that were determined by SAM analysis as having significantly different concentrations between Norm and Alsen for each treatment (Control, 9F1, Gz3639 and Gzt40) regardless of CO_2 level are depicted as separate heat maps. Metabolites that have significant concentration difference between Norm and Alsen for all treatments including control are indicated with a blue circles. Metabolites that are common between the DON^+ treatments (9F1 and Gz3639) are indicated with a red line. Red circles indicate metabolites that are in both DON^- (Gzt40) and DON^+ treatments but not in the control. Metabolites that provide the most accurate classification for control Norm and Alsen samples are designated with a red "X" (also in Supplementary Figure 5). In each group metabolites have been hierarchically clustered indicating similarities in behavior. Data is normalized across samples and metabolites for each group prior to SAM.

Figure 6. Metabolites with significant concentration differences at $1xCO_2$ vs $2xCO_2$. A. Relative concentration of metabolites that are significantly different at $1xCO_2$ (blue line) and $2xCO_2$ (red line) based on ANOVA analysis of all samples for all treatment groups. The metabolites are ordered by statistical significance based on ANOVA F-values provided in the table. Bars indicated standard variation across all samples in all treatment groups. B. Metabolites with significantly different concentrations between samples grown under $1xCO_2$ and $2xCO_2$ with respect to different treatments (control, 9F1, Gz3639, or Gzt40). PCA subplots show major variances (PC1 and PC2) for samples when analyzing concentrations of only the select metabolites with red showing samples grown at $2xCO_2$ and blue indicated samples grown at $1xCO_2$. Metabolites that are more abundant in plants at $2xCO_2$ relative to $1xCO_2$ are highlighted in red. Metabolites that are significantly affected by CO_2 in both Norm and Alsen wheat for a given treatment are highlighted in blue. Black and red X mark metabolites discussed in the text.

Supplementary Figures

Supplemental Figure 1. Spectra of metabolites used for quantification from 1D ^1H measurements. Shown spectra are obtained from HMDB in the raw format and preprocessed (including apodization, phasing and baseline correction) in house using MestReNova 11.0. Subsequently spectra were aligned to the NMR reference trimethylsilylpropionate that was added to all experimental samples. Metabolite concentrations are shown relative to the concentration of trimethylsilylpropionate scaled in this representation to be 1.

Supplemental Figure 2. PCA of NMR measurements and metabolite quantification for samples grouped by treatment. Difference in metabolic profiles of Norm and Alsen wheat when treated with *Fg* is apparent with major difference in DON^+ (9F1 and Gz3639) and smaller but still

observable difference in the DON$^-$ Gzt40 strain. Close agreement in the sample separation in PCA results when analyzing spectra and quantified data is apparent. Spectra have been normalized using NMR reference trimethylsilylpropionate and relative concentrations of metabolites obtained using multivariate linear regression have been normalized to norm 1. Methanol peak has been removed from analysis.

Supplemental Figure 3. Relative concentrations of all quantified metabolites for all NMR spectra shown as average values and standard deviations for treatments and CO_2 concentrations. Red bars indicated Alsen and blue bars indicate Norm.

Supplemental Figure 4. Hierarchical clustering of all samples and all quantified metabolites following scaling over all samples and metabolites. Outlined are samples belonging to Norm, Alsen and different treatments. Samples at different CO_2 levels are not separated by this level of clustering.

Supplemental Figure 5. Analysis of metabolic markers of resistance in the untreated plants with sample separation presented with PCA. Metabolite concentrations are shown relative to the concentration of trimethylsilylpropionate scaled in this representation to be 1. Table shows ANOVA F-values for the selected metabolites as determined in Orange.

Supplemental Figure 6. SAM analysis of major metabolic changes in Alsen wheat following treatment with 9F1 and Gz3639 wheat relative to control. Delta value shows thresholds for significance of the selected features.

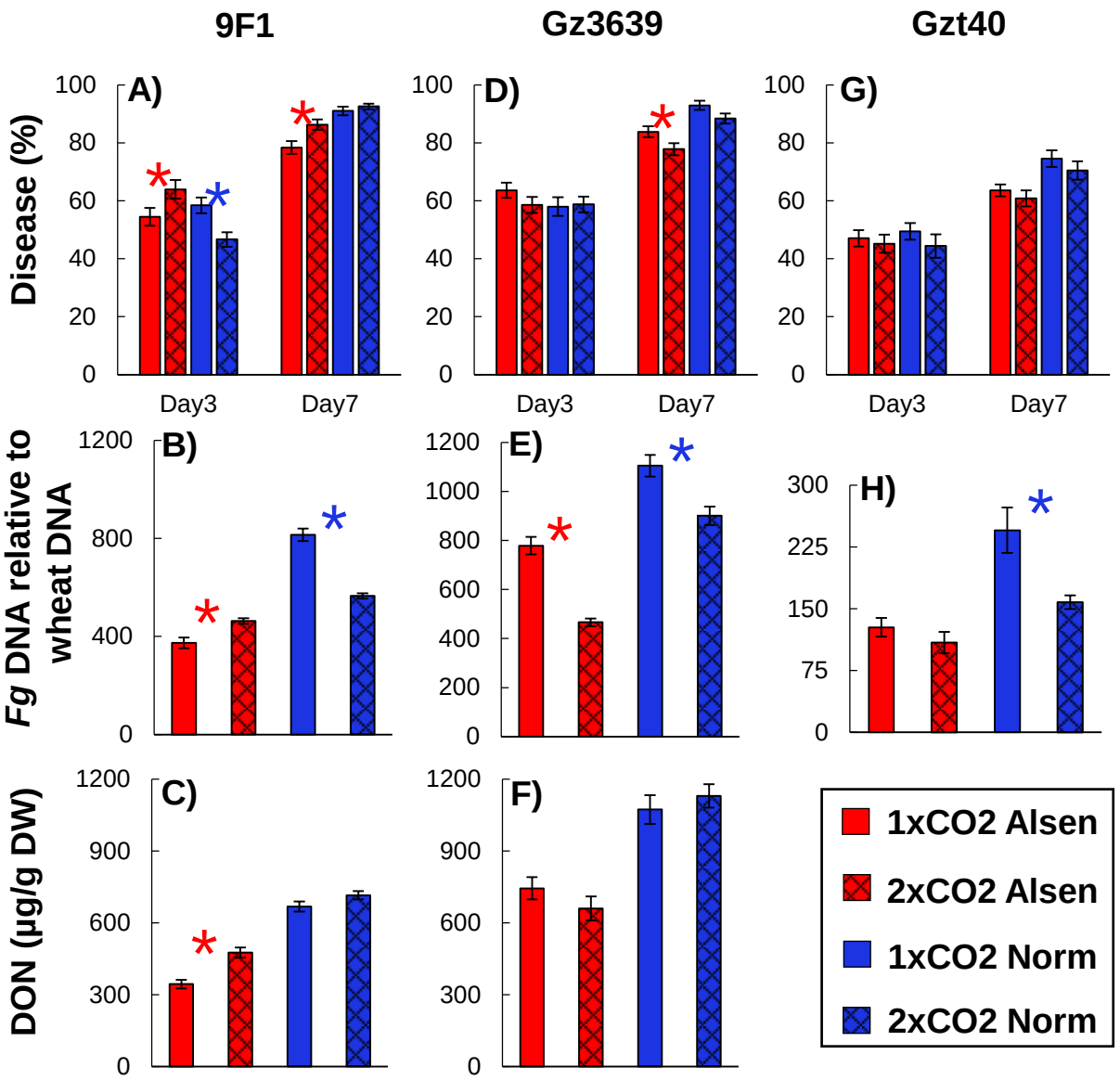

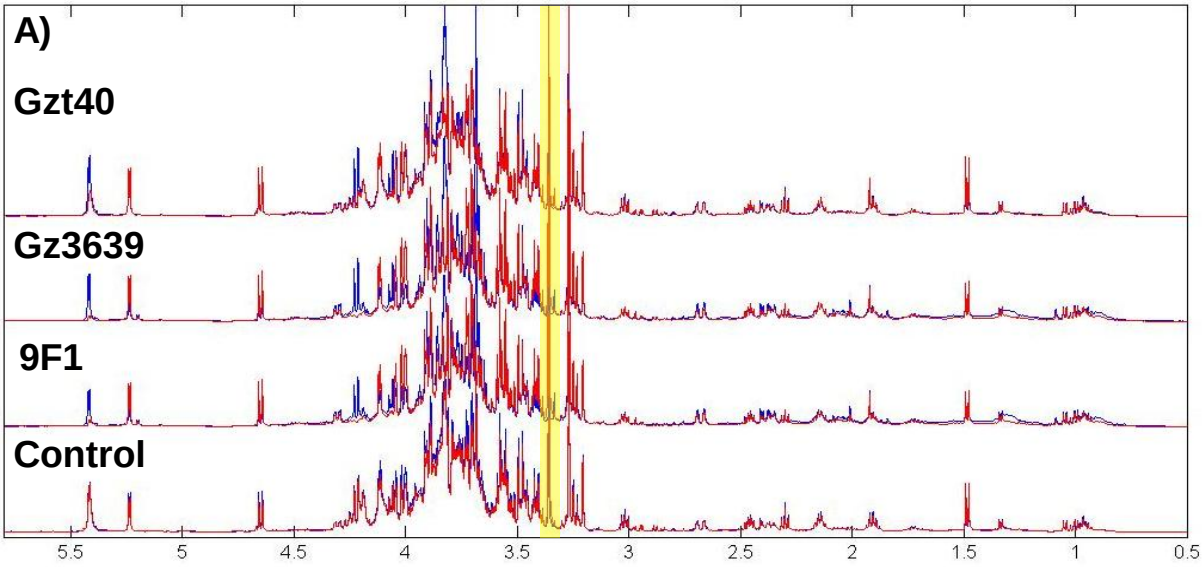

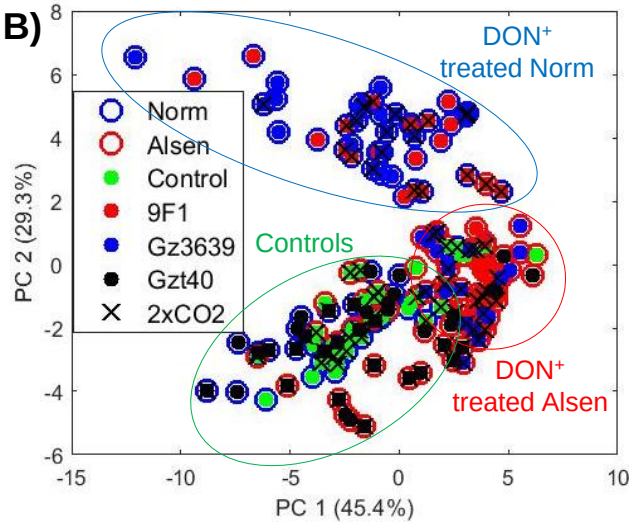

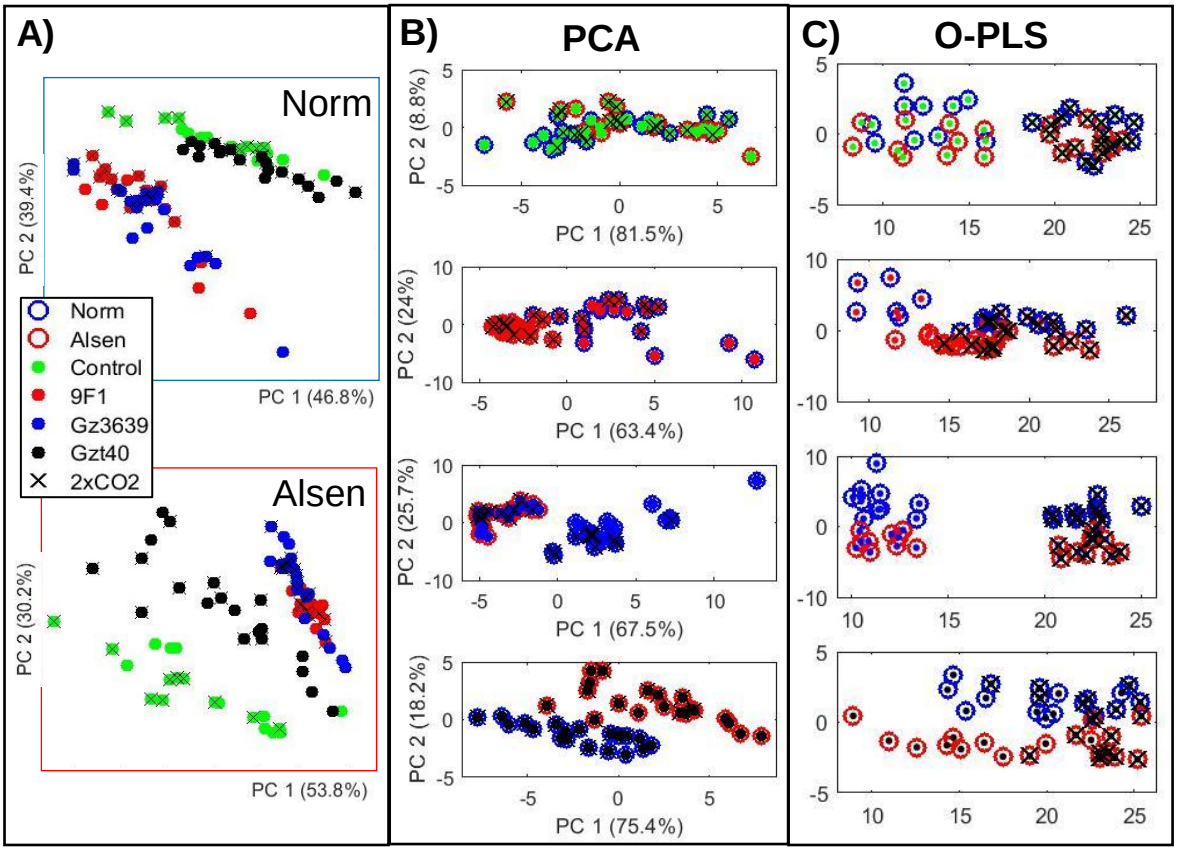

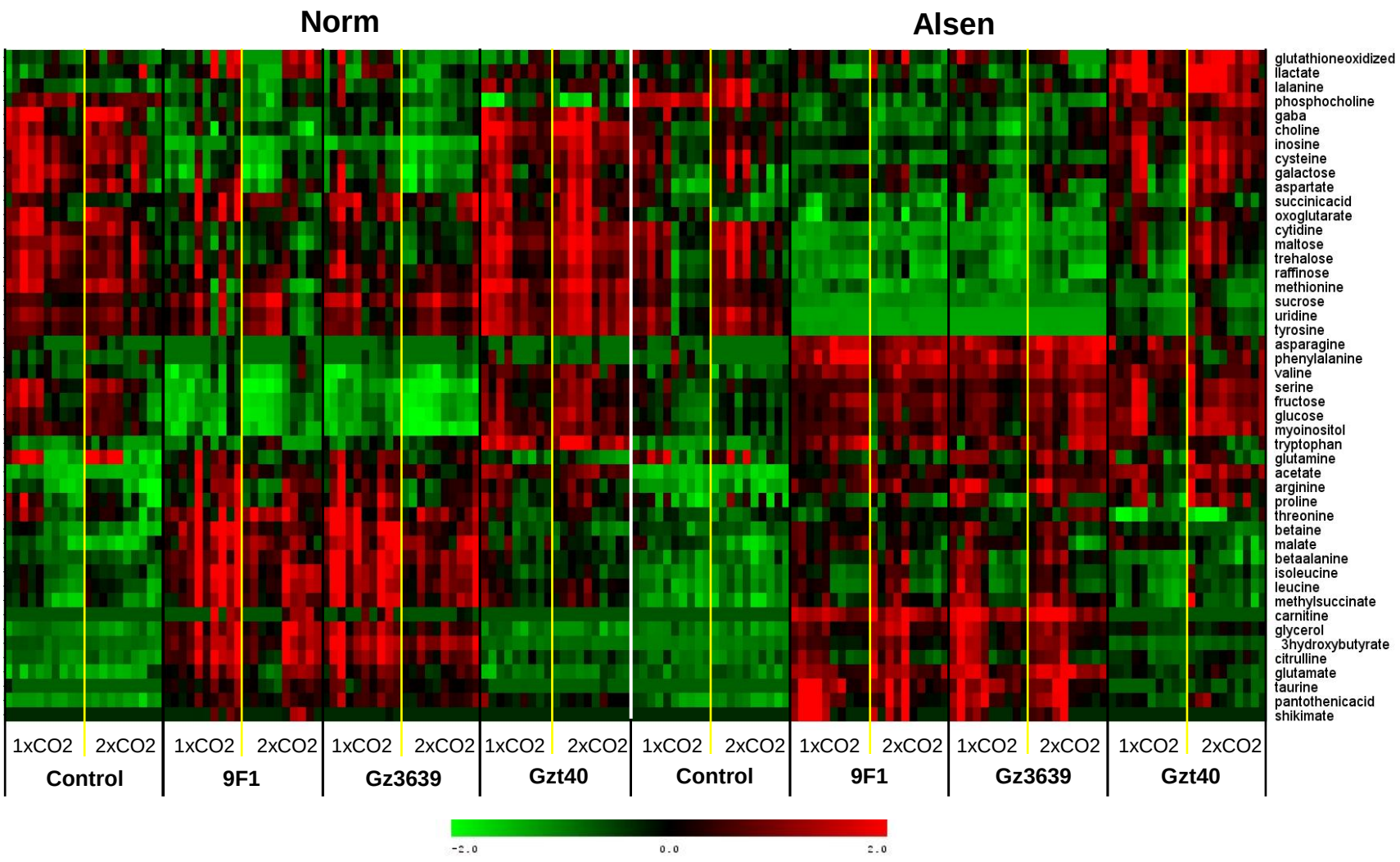

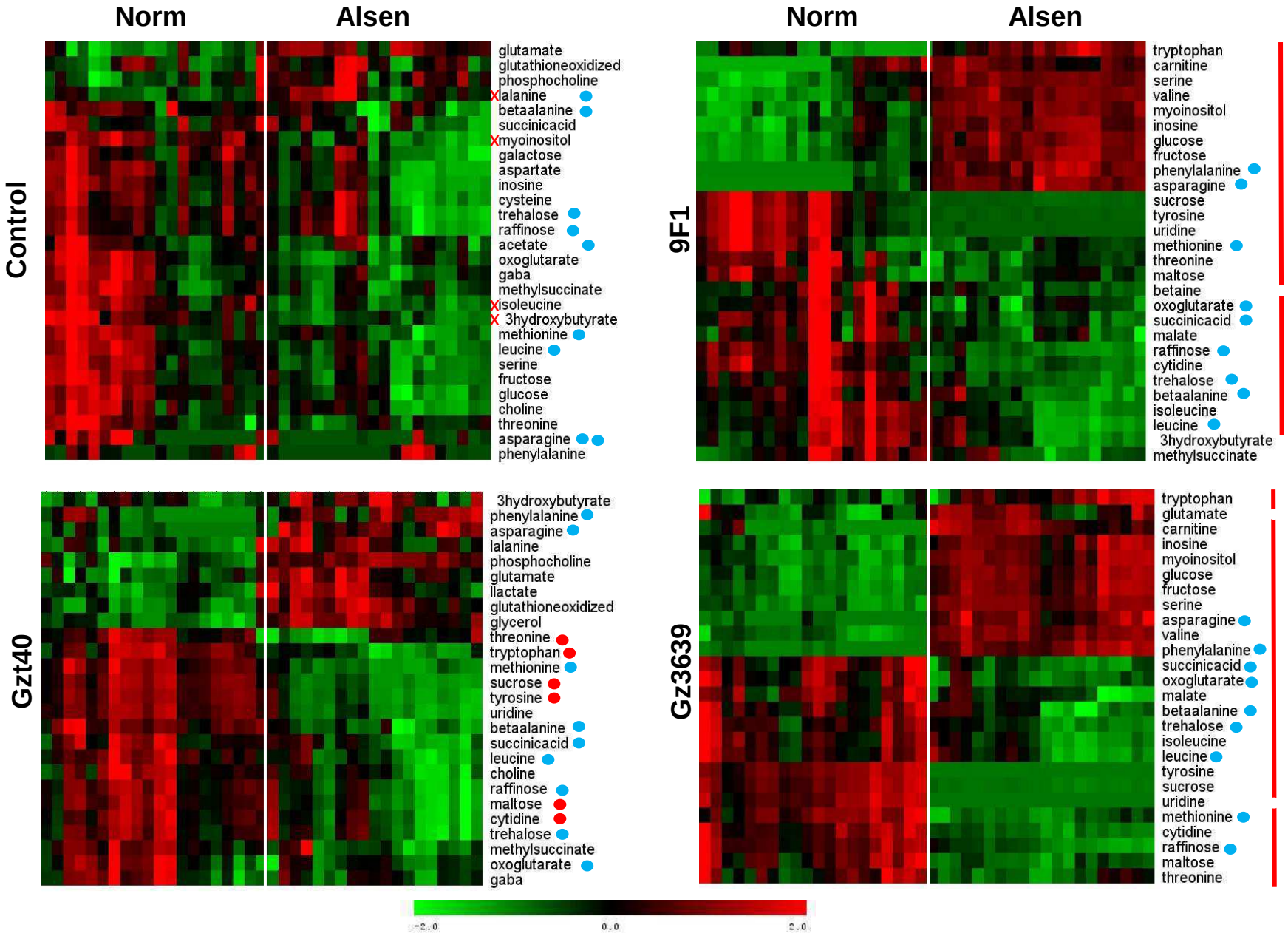

A)

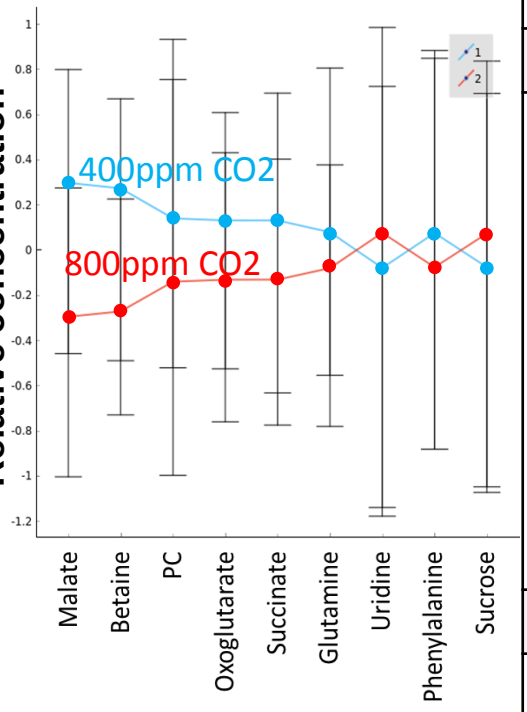

Metabolite	ANOVA F-value (Orange)
malate	12.025
betaine	5.908
PC	4.168
oxoglutarate	2.32
succinicacid	1.6
glutamine	1.6
uridine	0.46
phenylalanine	2.73
sucrose	0.884

B)

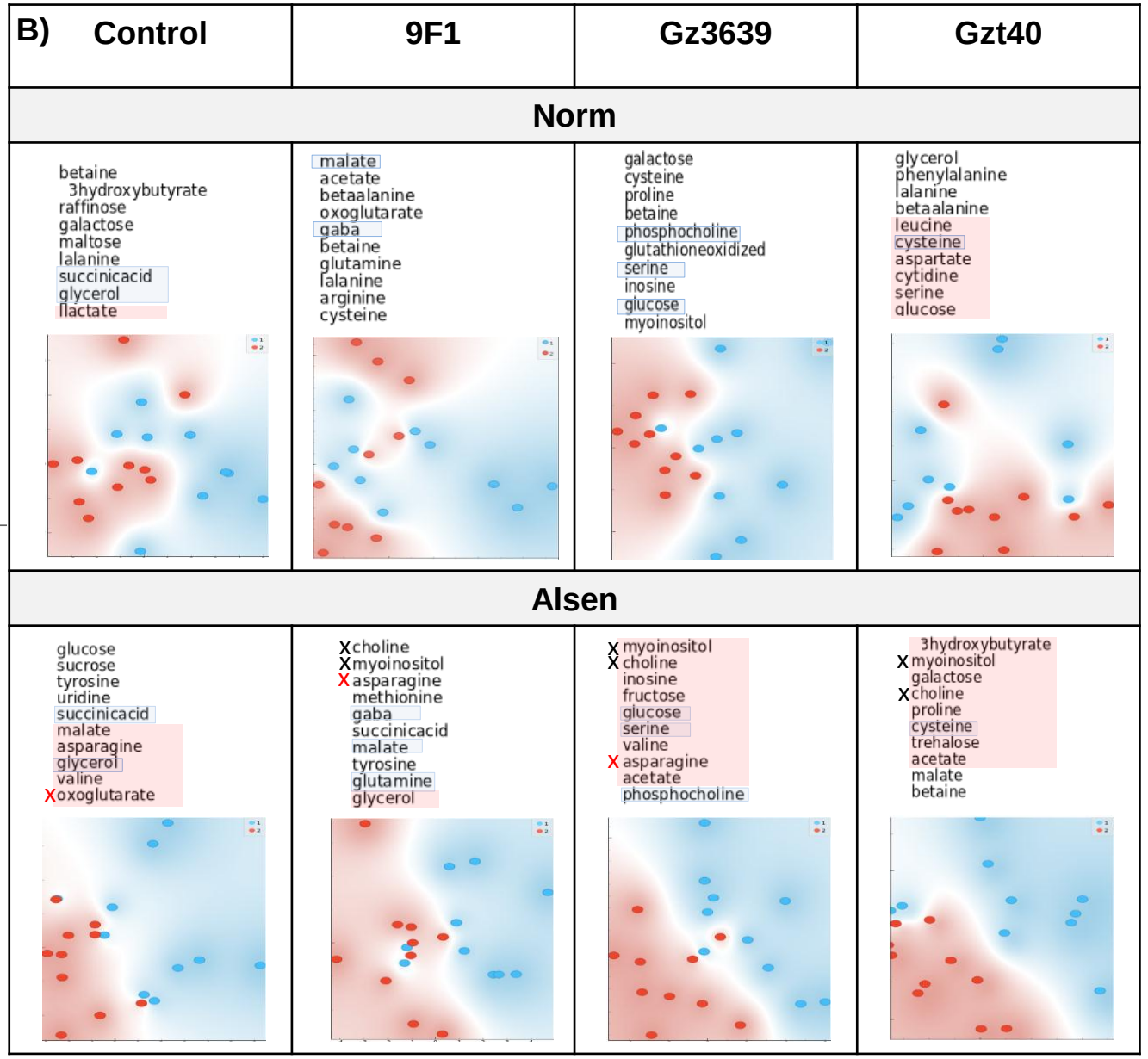

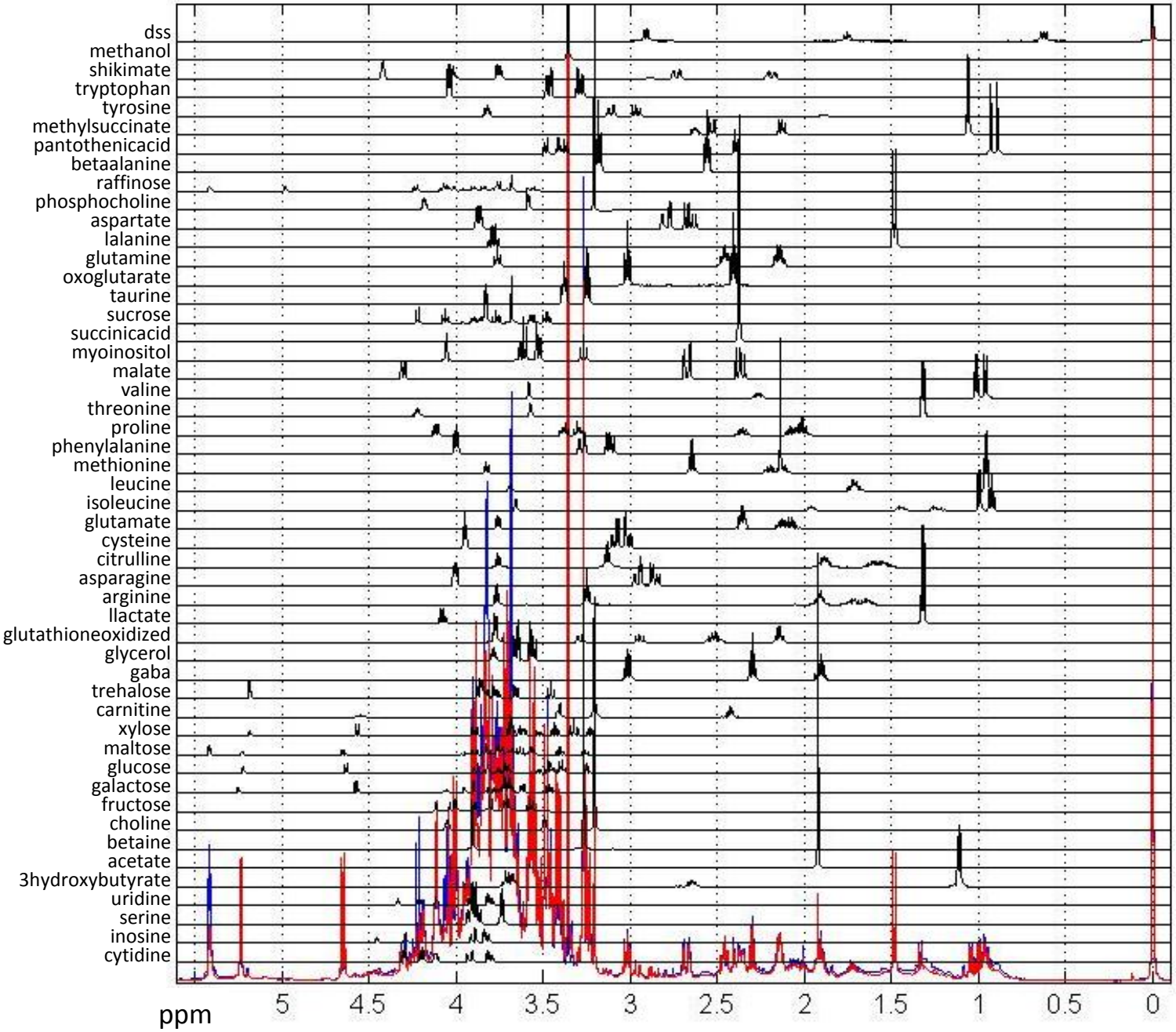

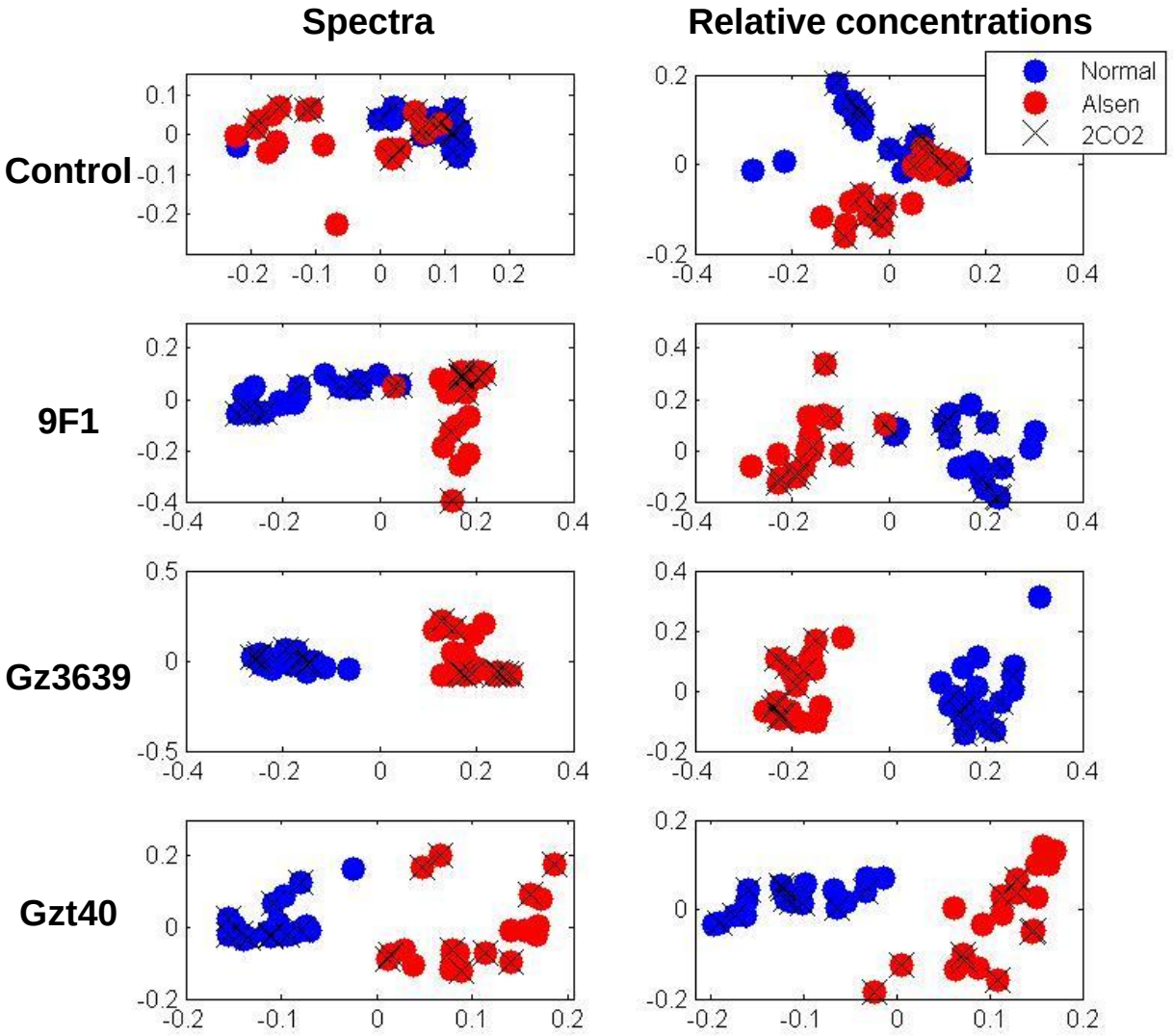

Carbohydrate pathway metabolites

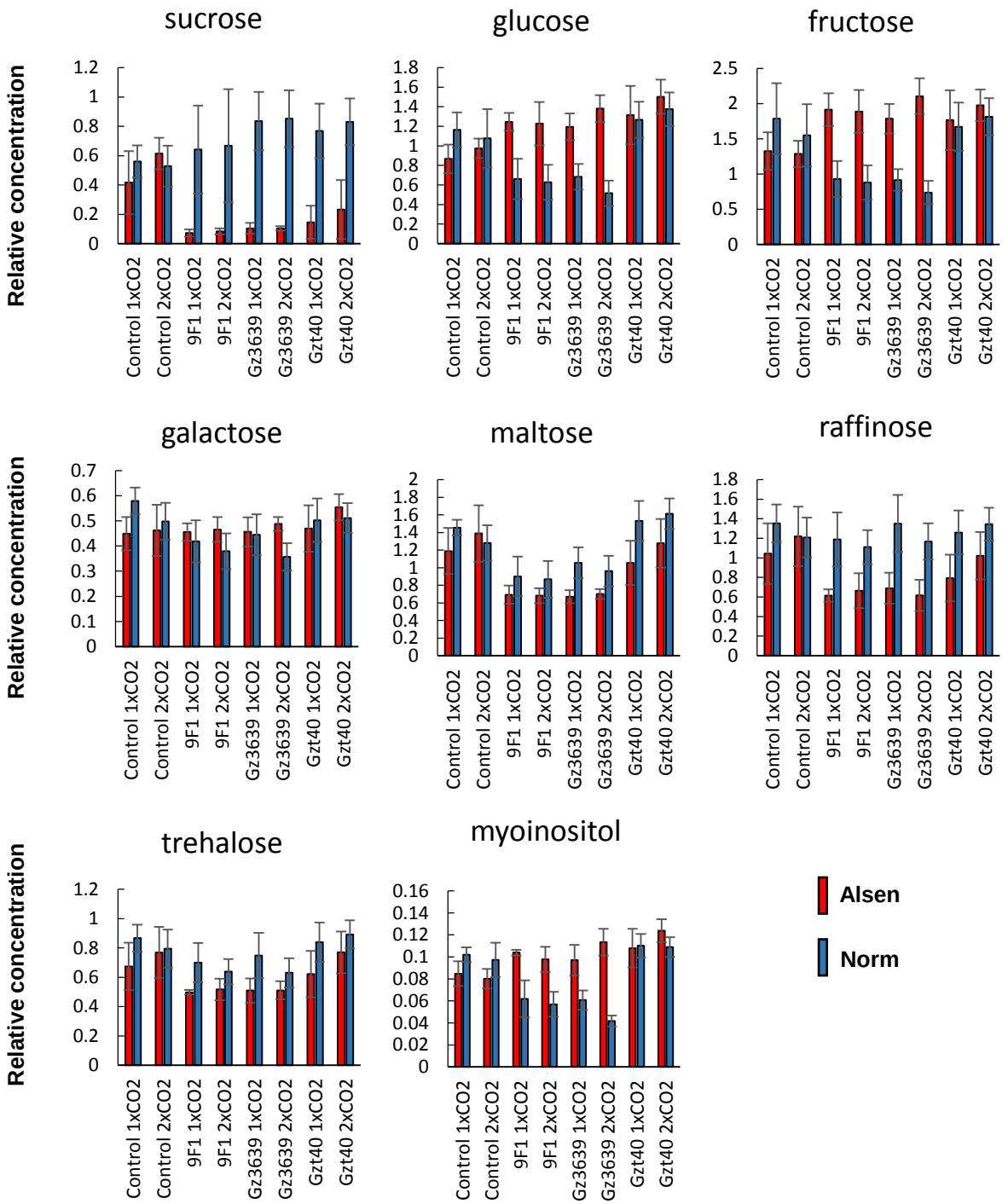

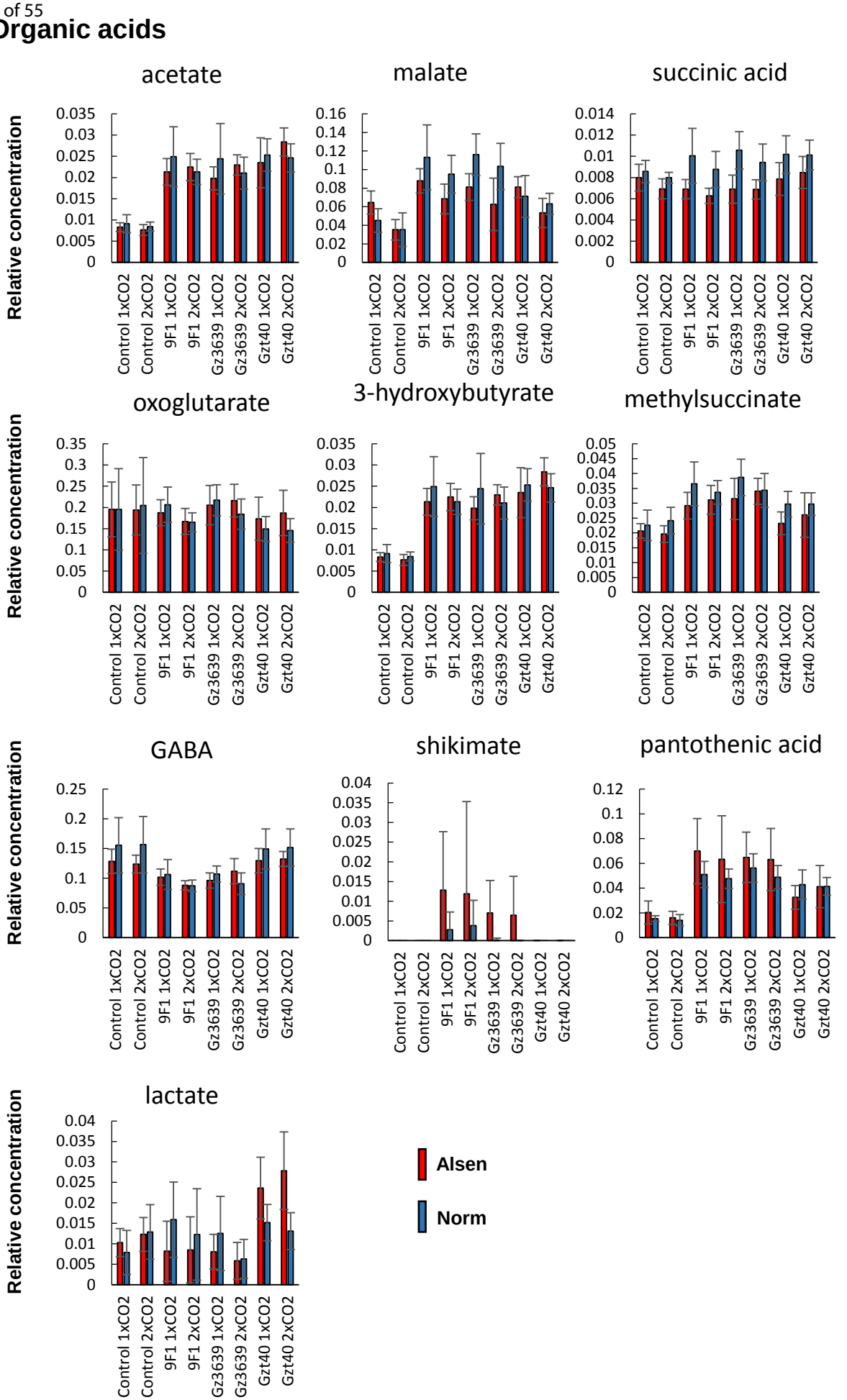

Amino Acids and derivatives

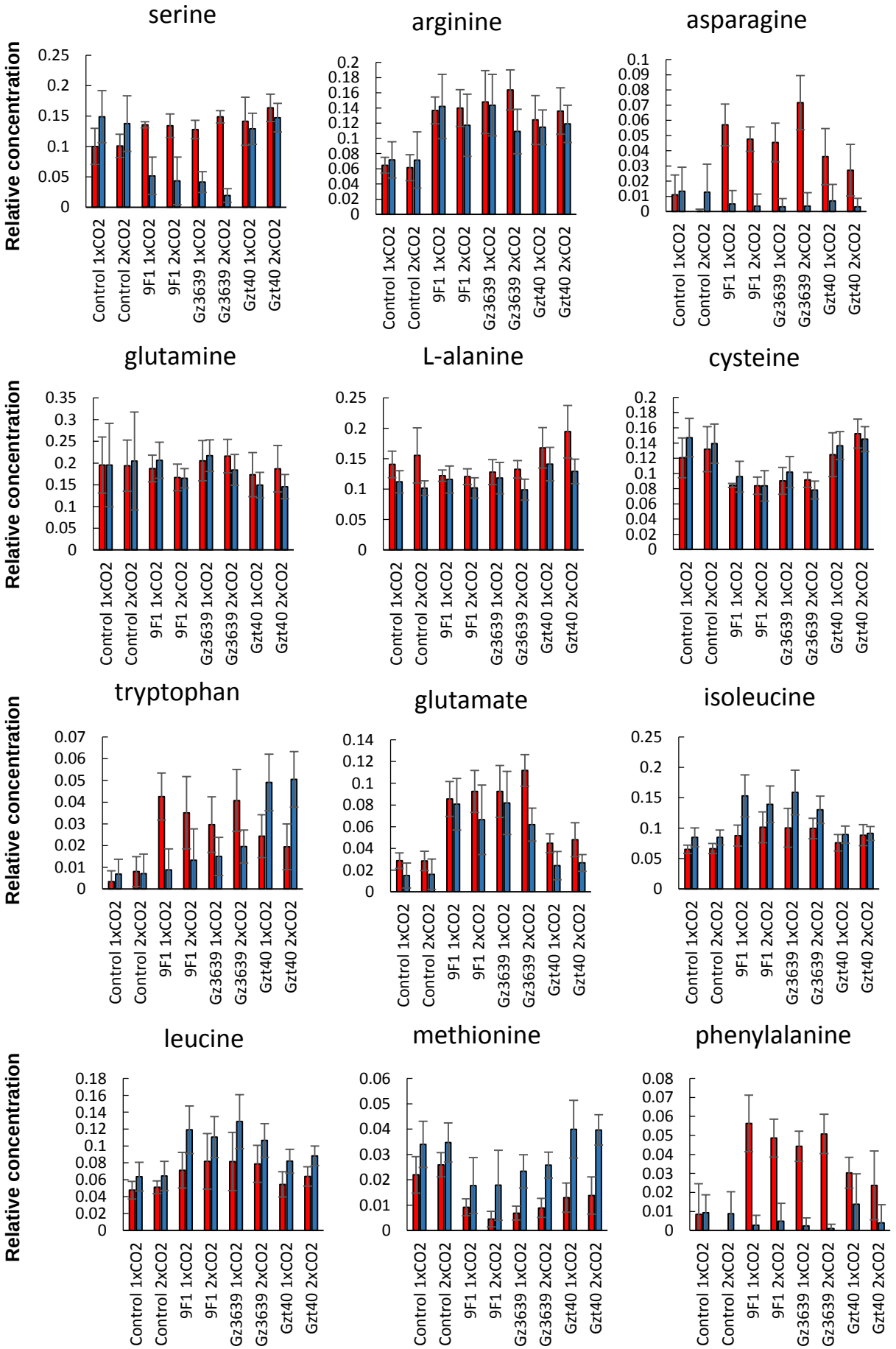

Amino Acids and derivatives

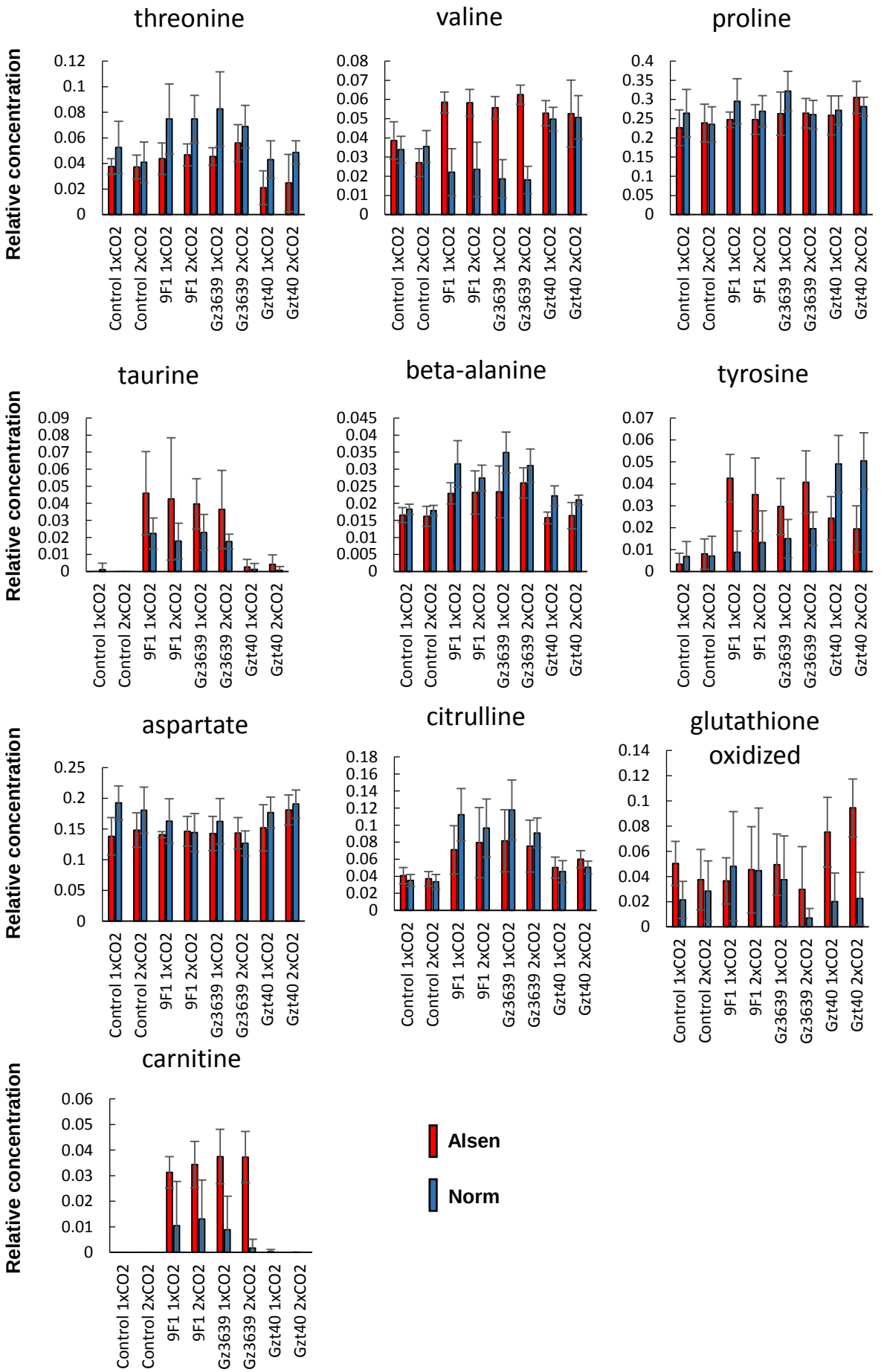

Others

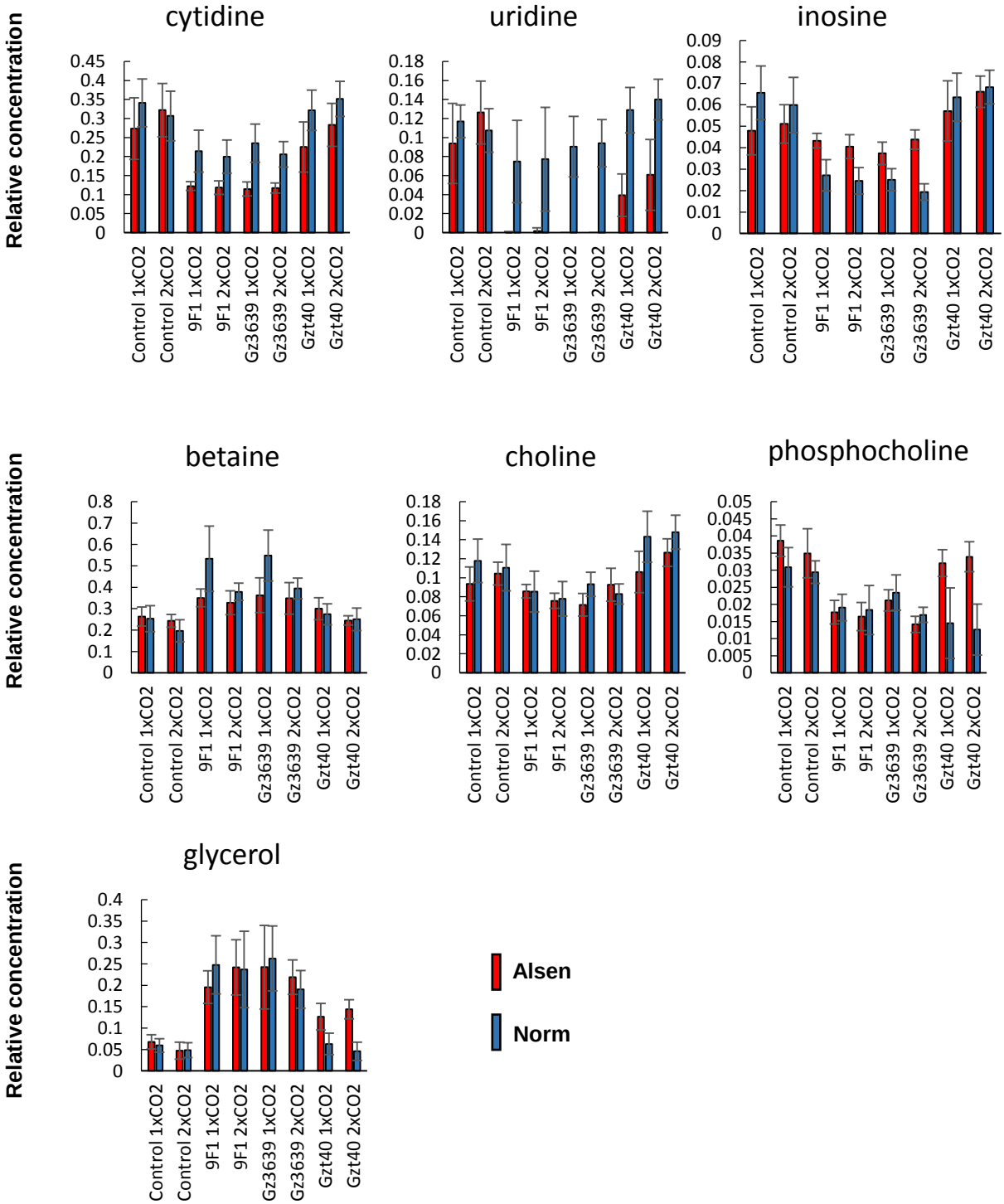

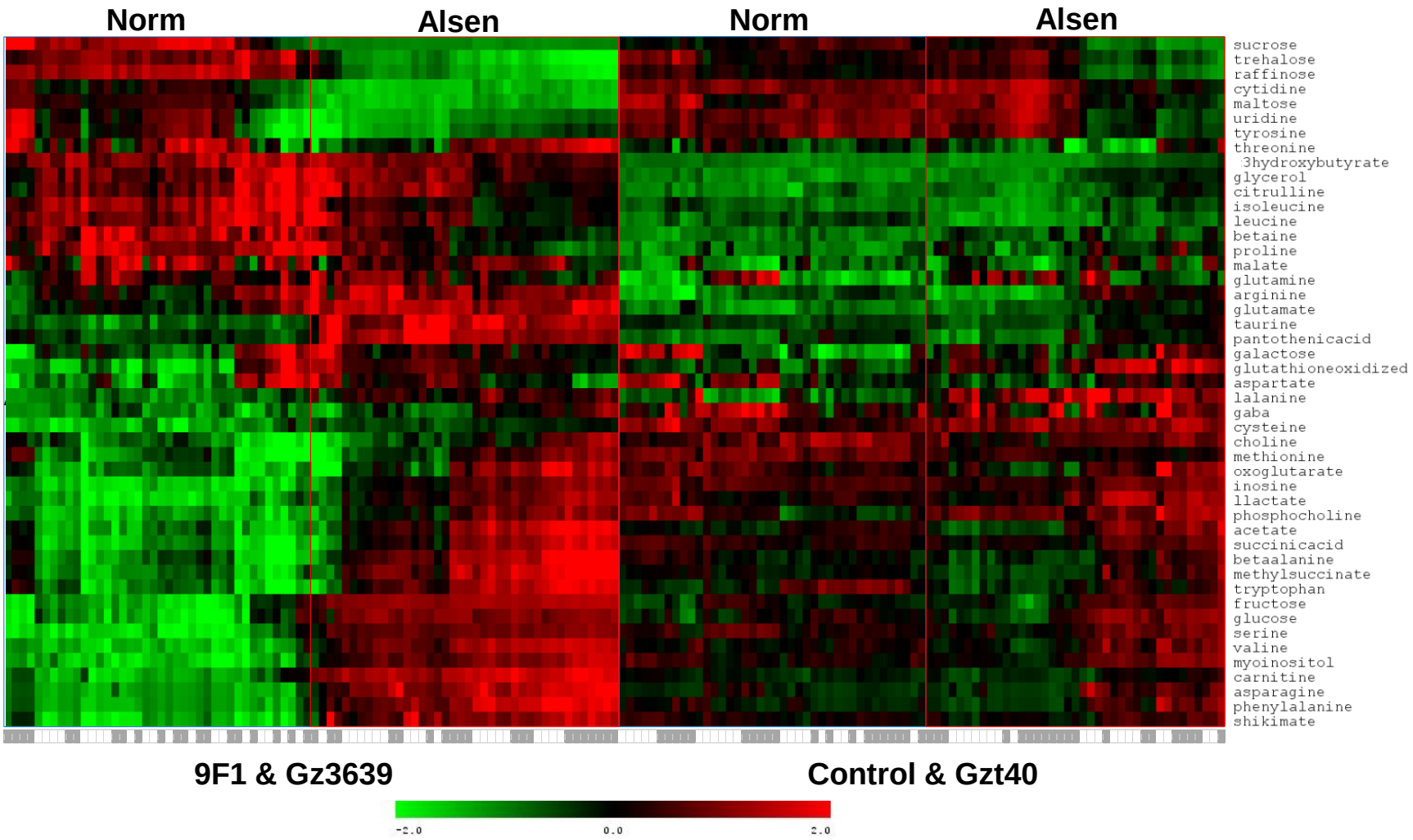

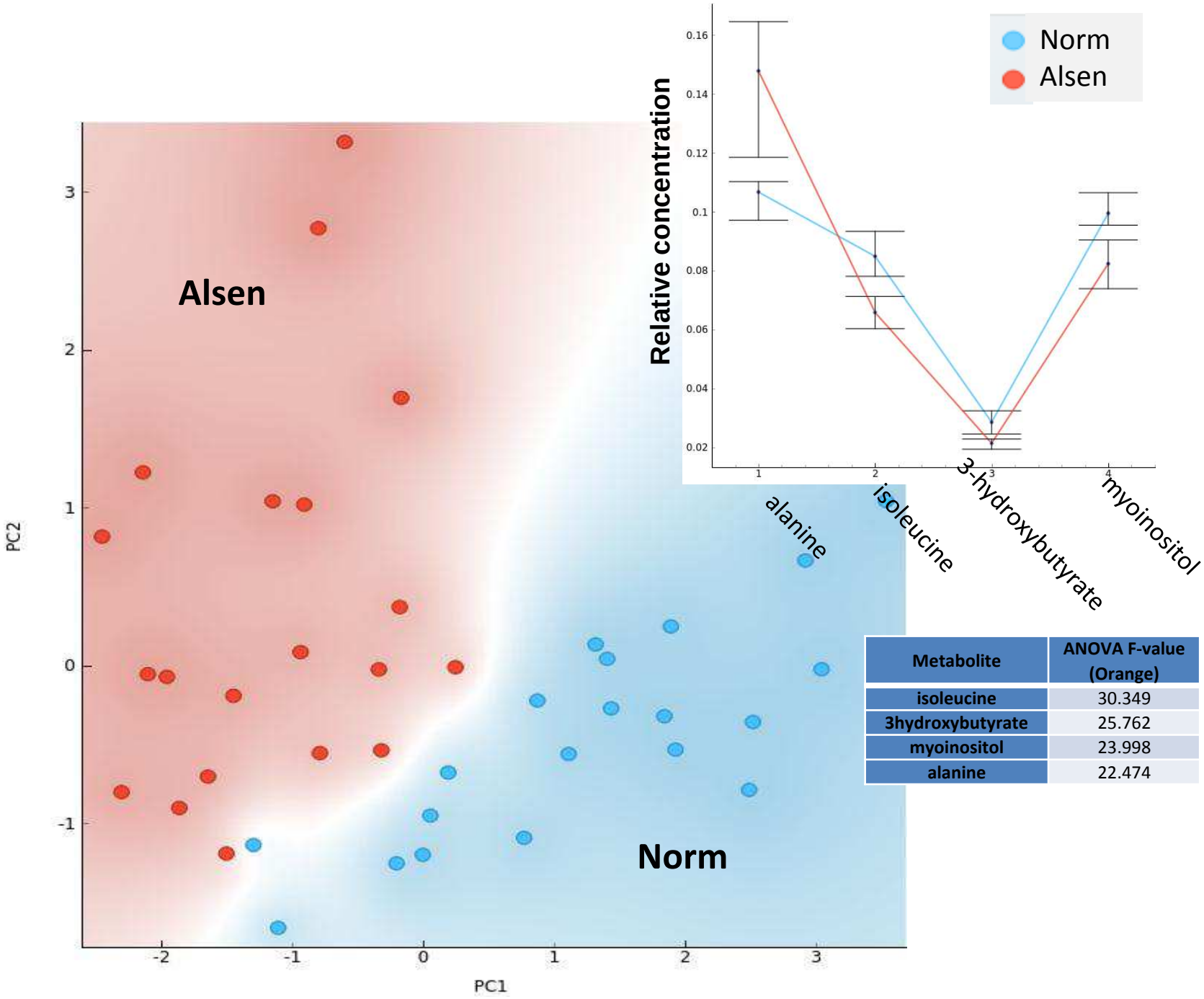

Metabolite	ANOVA F-value (Orange)
isoleucine	30.349
3hydroxybutyrate	25.762
myoinositol	23.998
alanine	22.474

	Control v.s. 9F1	Control v.s. Gz3639	Control v.s. Gzt40
1xCO2	Delta=4.5	Delta=4.2	Detla=2.7
2xCO2	Delta=4.6	Delta=6.4	Delta=3.1